Dimer-monomer transition defines a novel hyper-thermostable peptidoglycan hydrolase mined from bacterial proteome

Li Zhang[1,#], Fen Hu[2,#], Zirong Zhao[1,#], Xinfeng Li[3], Mingyue Zhong[3], Jiajun He[1], Fangfang Yao[4], Xiaomei Zhang[1], Yuxuan Mao[1], Hongping Wei[3], Jin He[1,*], Hang Yang[3,5,6,*]

[1]National Key Laboratory of Agricultural Microbiology & Hubei Hongshan Laboratory, College of Life Science and Technology, Huazhong Agricultural University, Wuhan 430070, China.

[2]Key Laboratory of Gastrointestinal Cancer (Fujian Medical University), Ministry of Education, Department of Etiology, School of Basic Medical Sciences, Fujian Medical University, Fuzhou 350002, China.

[3]Key Laboratory of Virology and Biosafety, Wuhan Institute of Virology, Chinese Academy of Sciences, Wuhan 430071, China.

[4]The State Key Laboratory Breeding Base of Basic Science of Stomatology (Hubei-MOST) & Key Laboratory of Oral Biomedicine, Ministry of Education, School of Stomatology, Wuhan University, Wuhan 430079, China.

[5]University of Chinese Academy of Sciences, Beijing 100049, China.

[6]Hubei Jiangxia Laboratory, Wuhan 430200, China.

#those authors contributed equally to this work.

For correspondence: *Jin He: hejin@mail.hzau.edu.cn; *Hang Yang: yangh@wh.iov.cn;

Running title: Mining of PHAbs from bacterial proteome

Abstract

Phage-derived peptidoglycan hydrolases (i.e., lysins) are considered a promising alternative to traditional antibiotics due to their low risks of resistance and unique mechanisms of action. However, the discovery of these enzymes is often hampered by limited source of available phage genomes. Herein, we report a new strategy to mine novel peptidoglycan hydrolases from bacterial proteomes by lysin-derived antimicrobial peptide-primed screening. As a proof-of-concept, five novel peptidoglycan hydrolases from the *Acinetobacter baumannii* proteome (PHAb7-PHAb11) were identified using PlyF307 lysin-derived peptide as a template. PHAb10 and PHAb11 showed potent bactericidal activity against a variety of pathogens even after treatment at 100°C for 1 hour, while the other three were thermosensitive. We solved the crystal structures of PHAb8, PHAb10, and PHAb11 and unveiled that hyper-thermostable PHAb10 underwent a unique folding-refolding thermodynamic scheme mediated by the dimer-monomer transition, while thermosensitive PHAb8 formed a monomer. Two mouse models of bacterial infection further demonstrated the safety and efficacy of PHAb10. Altogether, our antimicrobial peptide-primed strategy provides new clues for the discovery of novel antimicrobial drugs with therapeutic promise.

Keywords: Phage lysin, peptidoglycan hydrolase, bacterial proteome, hyper-thermostability, broad host range

58 **Introduction**

59 Despite decades of concerted action from all over the world, antimicrobial resistance remains
60 a growing global threat nowadays (1). The unreasonable use of antimicrobial agents in human,
61 livestock, industrial agriculture, and aquaculture is the main reason for the uncontrollable
62 spread and accumulation of antimicrobial resistance (2). Abuse and overuse of antimicrobial
63 agents leads to the accumulation of these antimicrobials in environment, eventually increasing
64 the chances of evolution of bacterial pathogens to acquire resistance (3, 4). Therefore, the
65 concept of "One Health" has been proposed to address the alarming levels of antimicrobial
66 resistance (5, 6). In recent decades, the number of bacteria resistant to first-line drugs has been
67 increasing, and the number of bacteria resistant to second- or third-line drugs has also increased.
68 Some of them have even been identified as multi-drug resistant, extensively drug resistant, or
69 pan-drug resistant isolates (7). For example, methicillin-resistant *Staphylococcus aureus*,
70 vancomycin-resistant *S. aureus*, vancomycin-resistant enterococcus, colistin-resistant
71 Enterobacteriaceae, third generation of cephalosporin-resistant *Escherichia coli* and *Klebsiella*
72 *pneumoniae*, carbapenem-resistant *E. coli*, *K. pneumoniae*, and *Pseudomonas aeruginosa*, and
73 multi-drug *Acinetobacter baumannii* cause a severe threat and are responsible for most of the
74 morbidity and mortality in modern clinical practice (8). Certainly, the global medical need for
75 novel antimicrobial has yet to be fully addressed.

76 Recently, many attempts have been made to develop novel antimicrobial drugs with different
77 targets or mechanisms of action than traditional antibiotic (9). These antibacterial pipelines
78 include small molecules with new targets such as ribosomal binding sites, membrane and cell
79 wall, gene interference, and metabolism (10, 11); antibacterial vaccines, antibodies and
80 antibody-drug conjugates targeting conserved antigens of specific pathogen (12); phages and
81 phage-derived peptidoglycan hydrolases, i.e., lysins that can lysis susceptible bacteria
82 individually or as a cocktail (13, 14); microbiome-modulating therapies targeting bacterial
83 colonization environments (primarily the intestine) (15); anti-virulent agents that target
84 different bacterial virulence factors, such as quorum sensing, biofilm formation, adhesion,
85 multiple regulators and persisters (16); potentiators that alone have no or low antibacterial
86 activity but otherwise restore or enhance the activity of another antibacterial agent (17);
87 immunomodulators that modulate the outcome of bacterial infection *via* a host-directed

88 approaches (18, 19); and nanobiotics that have antibacterial capacity through the generation of
89 reactive oxygen species, cell membrane permeation, triggering DNA damage or interrupting
90 transmembrane electron transport (20). In addition, drug repurposing, the strategy of
91 repurposing non-antimicrobial drugs to treat bacterial infections, also represents a time-saving
92 and cost-effective approach to antimicrobial discovery (21, 22). While these approaches hold
93 particular promise and advantages in accelerating discovery of potential compounds for clinical
94 studies, they nevertheless have substantial obstacles to overcome. The common denominator is
95 the lack of efficient hit-to-lead discovery methods.
96 Recent advances in metagenomics, artificial intelligence and synthetic biology have allowed
97 and inspired a renaissance in research into novel antimicrobial agent discovery. There is a trend
98 towards mining encrypted antimicrobial agents, especially peptides, through algorithms
99 coupled with biophysical feature selection that rely on rational design, machine learning, or
100 artificial intelligence-based tools derived from big data, such as the human proteome and
101 intestinal microbiome (23, 24), human and environmental metagenomics (25), protein sequence
102 space (26), and virtual prediction library and display (27, 28). It is not fully known yet how this
103 event will affect the evolutionary arms race between bacteria and the agents designed to kill
104 them, and consequently the entire field of antimicrobial resistance. But it is clear that novel
105 antimicrobial agents with relatively low risk of resistance will be crucial.
106 Abundant evidence has showed that bacterial peptidoglycans are a promising target for the
107 development of antimicrobial agents with low risk of inducing resistance. A well-documented
108 example in this regard is the peptidoglycan hydrolases, also known as lysins, derived from
109 phages. In recent years, lysins have been shown to be efficient alternatives to traditional
110 antibiotics for infections caused by Gram-positive bacteria in various animal models (14, 29).
111 Encouragingly, several lysins targeting *S. aureus* has been evaluated in clinical trials (30).
112 However, the discovery of lysins against Gram-negative pathogens meeting the needs described
113 in the WHO list of priority pathogens is still in its infancy (31, 32). Additionally, the discovery
114 of phage-derived peptidoglycan hydrolases has also been hampered by limited sources of
115 published phage genome data. Although not yet tested extensively, recent progress in lysins
116 targeting on Gram-negative bacteria have demonstrated a clue linking antibacterial activity to
117 their internal antimicrobial peptides, by which lysins cross the bacterial outer membrane and

118 contact its underlying peptidoglycan substrates (33-35). These observations led us to consider
119 whether it is feasible to mine novel antibacterial peptidoglycan hydrolases or their homologues
120 from bacterial proteomes by using lysin-derived antimicrobial peptide as template. As a proof-
121 of-concept, here we searched for novel peptidoglycan hydrolases from the *A. baumannii*
122 proteome database (PHAbs, Fig. S1) using the antimicrobial peptide P307 derived from
123 PlyF307 lysin (33) as a template. Two of them (PHAb10 and PHAb11) were found to be
124 hyperthermally stable even after treatment at 100°C for 1 hour, which might be mediated by a
125 unique monomer-dimer swapping. Furthermore, both were active against a wide variety of
126 clinically relevant bacteria *in vitro* and in mouse infection models. This observation supports
127 our hypothesis that antimicrobial peptide-primed mining strategy was feasible for discovering
128 novel peptidoglycan hydrolases from bacterial proteome with high bactericidal activity and
129 ideal physicochemical properties.
130

131 **Results**

132 **Screening of putative peptidoglycan hydrolases from the *A. baumannii* proteome based on**
133 **a lysin-derived antimicrobial peptide-primed mining strategy**

134 Since a variety of lysins active against Gram-negative bacteria are shown to harbor an N- or C-
135 terminal antimicrobial peptide, this led us to speculate that antimicrobial peptide would be used
136 as template to mine novel peptidoglycan hydrolases. To prove this hypothesis, P307, a well-
137 documented antimicrobial peptide against *A. baumannii* from PlyF307 lysin (33, 34), was used
138 as the template to mine putative peptidoglycan hydrolases from *A. baumannii* (PHAb) proteome
139 database publicly available in NCBI (Fig. 1a). Finally, 204 hits were identified and further
140 divided into 5 clades base on phylogenetic analysis. Clade I contained 162 hits with high
141 similarity (> 85%) to the AcLys lysin from *A. baumannii* 5057UW prophage (Fig. 1b), and
142 clade II-V contained 42 hits with relatively lower homology (40-77%) to each other (Fig. 1b
143 and Fig. S2a).
144 Due to the high similarity of amino acid sequences within each clade, we selected a putative
145 peptidoglycan hydrolase from each clade for further characterization by analyzing the
146 selectivity priority in evolution and the overall physicochemical properties (water solubility,
147 hydrophilicity, hydrophobicity, charge, flexibility, and rigidity) of each sequence *in silico*.
148 Finally, WP_065188953.1 from clade I, WP_0383495441.1 from clade II, KCY28522.1 from

clade III, WP_000109885.1 from clade IV, and WP_032023242.1 from clade V were shortlisted and renamed as PHAb11, PHAb10, PHAb9, PHAb8, and PHAb7, respectively, for further investigation (Fig. 1b). Further homology analysis revealed that these five peptidoglycan hydrolases showed great diversity with the structured AcLys lysin and the original PlyF307 lysin (Fig. S2b).

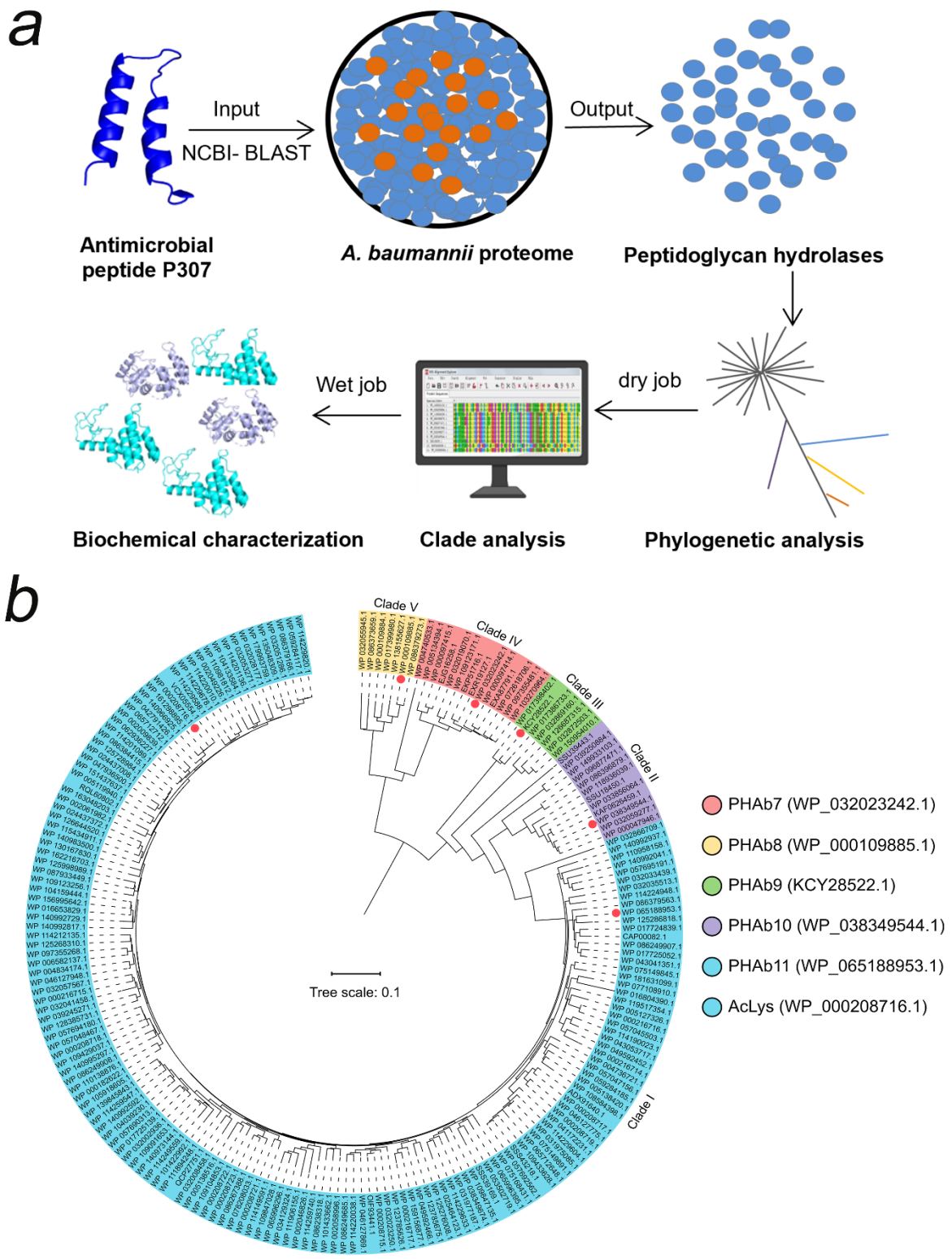

155 **Fig. 1 Screening of putative peptidoglycan hydrolases from the *A. baumannii* proteome.** (a)
156 Workflow for the development of an integrated system for peptidoglycan hydrolase screening. (b)
157 Phylogenetic analysis of putative peptidoglycan hydrolases from the *A. baumannii* proteome database.
158 Multiple sequence alignments are performed using MEGAX software with ClustalW algorithm, and the
159 Neighbor-joining method is used to construct a phylogenetic tree. Classified clades are labeled in
160 different colors and representative peptidoglycan hydrolases from each clade are pointed by colored
161 circles.
162

163 **PHAb10 and PHAb11 are highly thermostable peptidoglycan hydrolases with a broad-**
164 **spectrum of action**

165 To test the activity of these PHAbs, their coding sequences were chemically synthesized, cloned
166 to vector, and expressed in *E. coli* cells. As expected, all five PHAbs were well expressed as
167 soluble proteins in *E. coli* BL21(DE3) with high purity (Fig. S3a). Next, we examined the
168 hydrolytic activity of these 5 PHAbs on peptidoglycan derived from *A. baumannii* 3437 by halo
169 assay. Results showed that even at a low concentration of 2.5 μg/ml, all PHAbs formed clear
170 zones on autoclaved *A. baumannii* lawns (Fig. S3b), indicating that these PHAbs were active
171 against peptidoglycan from *A. baumannii*. To further confirm the ability of these PHAbs against
172 peptidoglycan from different bacteria, we measured the area of clear zones generated by
173 different concentrations of PHAbs on each lawn of two isolates of *A. baumannii*, *P. aeruginosa*,
174 and *E. coli*. Encouragingly, these PHAbs were active against peptidoglycans from all strains
175 tested and formed a clear halo (Fig. 2a). Among these PHAbs, PHAb10 and PHAb11 showed
176 larger size of clear zones under each concentration tested (Fig. 2a), indicating that these two
177 PHAbs might have stronger peptidoglycan hydrolyzing activity. To prove this, we further
178 evaluated the bactericidal activity of these PHAbs against each isolate of *A. baumannii*, *P.*
179 *aeruginosa*, and *E. coli* by a log-killing assay. Consistent with the halo assay, PHAb10 and
180 PHAb11 exhibited outstanding bactericidal activity against all strains tested, with a 3.5-4.6 log
181 reduction in viable bacterial counts after treatment for 1 hour with 50 μg/ml of each enzyme
182 (Fig. 2b). Like other lysins, the potent bactericidal activity of PHAb10 and PHAb11 was time-
183 dependent. After treatment with 50 μg/ml of either enzyme, a ~0.9 log reduction in viable *A.*
184 *baumannii* 3437 for both enzymes were observed within the first 30 seconds, with a substantial
185 reduction to 3.1 logs (from 6.0 log to 2.9 log) for PHAb10 and 2.5 logs (from 6.0 log to 3.5 log)
186 for PHAb11 after 15 minutes (Fig. 2c).

187 Since previous reports documented the diverse performance of lysins against Gram-negative
188 and Gram-positive bacterial species in exponential and stationary phases (33), we therefore
189 examined the bactericidal activity of PHAb10 and PHAb11 against different bacteria in
190 different growth phases. Interestingly, robust bactericidal activity was observed for both
191 enzymes in exponential and stationary phase cultures of *A. baumannii*, *P. aeruginosa*, *E. coli*,
192 *K. pneumoniae*, *S. suis*, and *E. faecalis* (Fig. 2d). It should also be noted that exponential
193 bacteria were more susceptible to these two enzymes than stationary bacteria, similar to
194 observations reported elsewhere (33). However, for *S. aureus*, detectable susceptibility to
195 PHAb11 was only observed in its exponential phase (Fig. 2d). In addition, PHAb10 and
196 PHAb11 exhibited dose-dependent killing against sensitive Gram-negative and Gram-positive
197 strains tested. Specifically, treatment with 6.25 μg/ml PHAb10 for 1 hour resulted in a ~3 log
198 reduction in *A. baumannii*, a ~2.7 log reduction in *P. aeruginosa*, a ~3 log reduction in *E. coli*,
199 ~1.08 log reduction in *K. pneumoniae*, and a ~0.94 log reduction in *S. suis*, and treatment with
200 6.25 μg/ml PHAb11 for 1 hour caused a ~2.8 log reduction in *A. baumannii*, a ~2.6 log reduction
201 in *P. aeruginosa*, a ~2.7 log reduction in *E. coli*, a ~0.69 log reduction in *K. pneumoniae*, a ~1.3
202 log reduction in *S. aureus*, and a ~2.15 log reduction in *S. suis* (Fig. 2e). Interestingly, *E. faecalis*
203 was more sensitive to PHAb10 and PHAb11, showing a ~3.8 log and a ~4.6 log reduction
204 respectively after treatment with 10 μg/ml of each enzyme for 1 hour (Fig. 2f).
205 To further confirm the bactericidal activity of PHAb10 and PHAb11, the susceptibility of
206 various clinical isolates such as *A. baumannii*, *P. aeruginosa*, *E. coli*, *K. pneumonia*, *S. aureus*,
207 and *E. faecalis,* as well as representative isolates of *S. dysgalactiae, S. agalactiae*, *S. pyogenes*,
208 *S. pneumoniae*, and *S. suis* to both enzymes were examined by log-killing assay. Our results
209 showed that all tested strains, whether antibiotic-resistant or not, were sensitive to PHAb10 and
210 PHAb11 (Fig. 2g-h). Importantly, Gram-negative bacteria were more sensitive to PHAb10, with
211 3.9-6.0 log reductions for *A. baumannii* isolates, 3.7-5.0 log reductions for *E. coli* isolates, 2.4-
212 4.3 log reductions for *P. aeruginosa* isolates, and 1.1-3.6 log reductions for *K. pneumoniae*
213 isolates (Fig. 2g). In contrast, PHAb11 was more bactericidal than PHAb10 against Gram-
214 positive bacteria, causing 1.8-4.3 log reductions for *S. aureus* isolates, 4.5-5.0 log reductions
215 for *E. faecalis* isolates, and 1.0-6.1 log reductions for various streptococcal strains (Fig. 2h).
216 Further biochemical characterization showed that PHAb10 and PHAb11 remained highly active
217 at pH 5.0-10.0, and the maximum bactericidal activity was observed at pH 7.0 for both enzymes
218 (Fig. S3c). Similar to other previously reported lysins (36, 37), PHAb10 and PHAb11 were
219 sensitive to NaCl and urea in a dose-dependent inhibitory manner (Fig. S3d). Surprisingly, both
220 enzymes retained outstanding bactericidal activity after heat treatment at temperature up to

100°C for 1 hour (Fig. 2i). Indeed, after 1 hour treatment at 100°C, the bactericidal activity was improved slightly for both enzymes. In contrast, PHAb7, PHAb8, and PHAb9 completely lost their activity after treatment at 70°C for 1 hour (Fig. S3e). Together, these observations showed that PHAb10 and PHAb11 were highly thermostable peptidoglycan hydrolases with a broad spectrum of action.

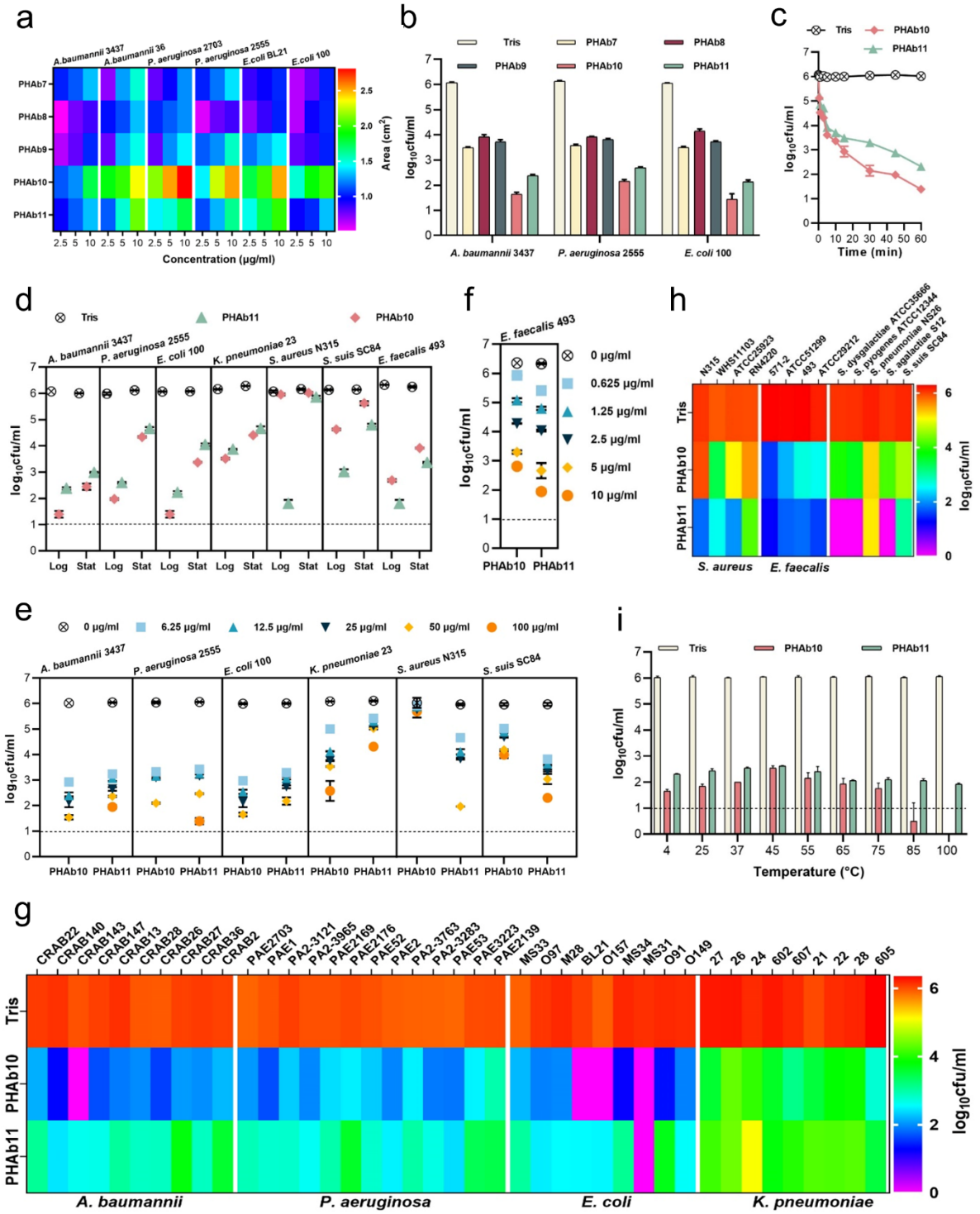

Fig. 2 PHAb10 and PHAb11 are highly thermostable peptidoglycan hydrolases with a broad-spectrum of action. (a) Heat map showing the halo size formed by different concentrations of

229 peptidoglycan hydrolases on different bacterial lawns. (b) Bactericidal activity of five peptidoglycan
230 hydrolases (50 μg/ml) in 20 mM Tris-HCl (pH 7.4) at 37°C for 1 hour against different exponential
231 bacteria. (c) Time-dependent bactericidal activity of 50 μg/ml PHAb10 or PHAb11 against exponential
232 *A. baumannii* in 20 mM Tris-HCl (pH 7.4). (d) Bactericidal activity of 50 μg/ml PHAb10 or PHAb11 in
233 20 mM Tris-HCl (pH 7.4) at 37°C for 1 hour against different bacteria in exponential and stationary
234 phases. (e-f) Dose-dependent bactericidal activity of PHAb10 and PHAb11 against multiple exponential
235 bacteria in 20 mM Tris-HCl (pH 7.4) at 37°C for 1 hour. (g-h) Susceptibility of various Gram-negative
236 (g) and Gram-positive (h) bacterial strains to PHAb10 and PHAb11. Exponential cultures of each
237 bacterium are treated with 50 μg/ml PHAb10 or PHAb11 for 1 hour at 37°C and residual viable bacterial
238 cells are counted by plating serial dilutions onto agar plates. For *E. faecalis*, 10 μg/ml of each
239 peptidoglycan hydrolase is used. (i) Thermal stability of PHAb10 and PHAb11. Each enzyme is stored
240 at different temperatures for 1 hour, cooled to room temperature, and then incubated with exponential
241 *A. baumannii* 3437 in 20 mM Tris-HCl (pH 7.4) at a final concentration of 50 μg/ml at 37°C for 1 hour.
242 Viable bacteria are counted after each treatment by plating serial dilutions on LB agar. Dash lines
243 represent the limit of detection and data below the limit of detection is not shown.

244

245 **Different action mechanisms of PHAb10 and PHAb11 in killing Gram-negative and**
246 **Gram-positive bacteria**

247 Due to the natural barrier of the outer membrane, several peptidoglycan hydrolases (i.e., lysins)
248 have been reported to have no or low bactericidal activity against Gram-negative bacteria in the
249 absence of outer membrane penetrating agents (31, 32, 38). However, for most of these lysins,
250 their activity is almost exclusively restricted to Gram-negative bacteria (39, 40), which casts
251 doubt on the mechanisms of action of PHAb10 and PHAb11 in killing both Gram-negative and
252 Gram-positive bacteria. Structural prediction analysis showed that PHAb10 contained a
253 putative lysozyme catalytic domain (amino acids 1-110, P10-Lys) and a C-terminal cationic
254 peptide (amino acids 111-149, P10-CP), whilst PHAb11 contained an N-terminal cationic
255 peptide with unknown function (amino acids 1-36, P11-NP), followed by a putative lysozyme
256 catalytic domain (amino acids 37-145, P11-Lys) and a C-terminal cationic peptide (amino acids
257 146-184, P11-CP) (Fig. 3a). Studies have shown that the cationic region of phage lysins can
258 facilitate their penetration into the outer membrane, thereby fulfilling their bactericidal activity
259 against Gram-negative bacteria (33, 35, 37). To examine whether it is the reason for the killing
260 ability of PHAb10 and PHAb11 against Gram-negative bacteria, we further analyzed *in silico*
261 the physicochemical properties of these putative cationic peptides harbored by these two
262 enzymes and found that all three peptides, that is, P10-CP, P11-CP, and P11-NP might act as
263 antimicrobial peptides (Table S1). Therefore, we synthesized these peptides and examined their

264 antibacterial activity by log-killing assay. As shown in Fig. 3b, we observed bactericidal activity
265 in P10-CP and P11-CP against *A. baumannii*, *P. aeruginosa*, *S. aureus*, and *E. faecalis* in both
266 the exponential and stationary phases. However, rare lytic activity was observed in P11-NP,
267 suggesting that a potential role for it in functions other than bactericidal activity. Notably, P11-
268 CP was more robust than P10-CP (Fig. 3b), which might be due to an extra positively charged
269 amino acid (i.e., Lysine) in P11-CP (Table S1). More importantly, the putative lysozyme
270 catalytic domains of two enzymes, P10-Lys, P11-Lys, and P11-N showed rare bactericidal
271 activity against all Gram-negative and Gram-positive bacteria tested (Fig. 3c-d), which
272 indicated that the antimicrobial peptides, namely P10-CP and P11-CP, were essential for the
273 bactericidal activity of both enzymes. Curiously, for unknown reasons, P11-C showed higher
274 bactericidal activity than the holoenzyme PHAb11 against all bacteria tested (Fig. 3d).
275 Considering the different targets of antimicrobial peptide and peptidoglycan hydrolase, we
276 further asked the killing mechanism of susceptible bacteria by PHAb10 and PHAb11. To this
277 end, we evaluated the effects of different truncations of PHAb10 and PHAb11 on different
278 bacteria by halo assay to test their peptidoglycan hydrolase activity. Results showed that
279 lysozyme-containing truncations from both enzymes showed hydrolytic activity only towards
280 peptidoglycan from Gram-negative bacteria but not from Gram-positive bacteria (Fig. 3e),
281 suggesting that the killing of Gram-positive bacteria by PHAb10 and PHAb11 is probably
282 mediated mainly by their internal antimicrobial peptides, i.e., P10-CP and P11-CP. Supporting
283 to this assumption, rare peptidoglycan hydrolytic activity was observed in P10-CP and P11-CP
284 (Fig. 3e). Altogether, these results suggested that the killing of Gram-negative bacteria by
285 PHAb10 and PHAb11 might be a combination of lysozyme-mediated peptidoglycan hydrolytic
286 activity and antimicrobial peptide-mediated outer membrane-disruption activity. However, their
287 bactericidal activity against Gram-positive bacteria was primed solely by their internal
288 antimicrobial peptides (Fig. 3f).

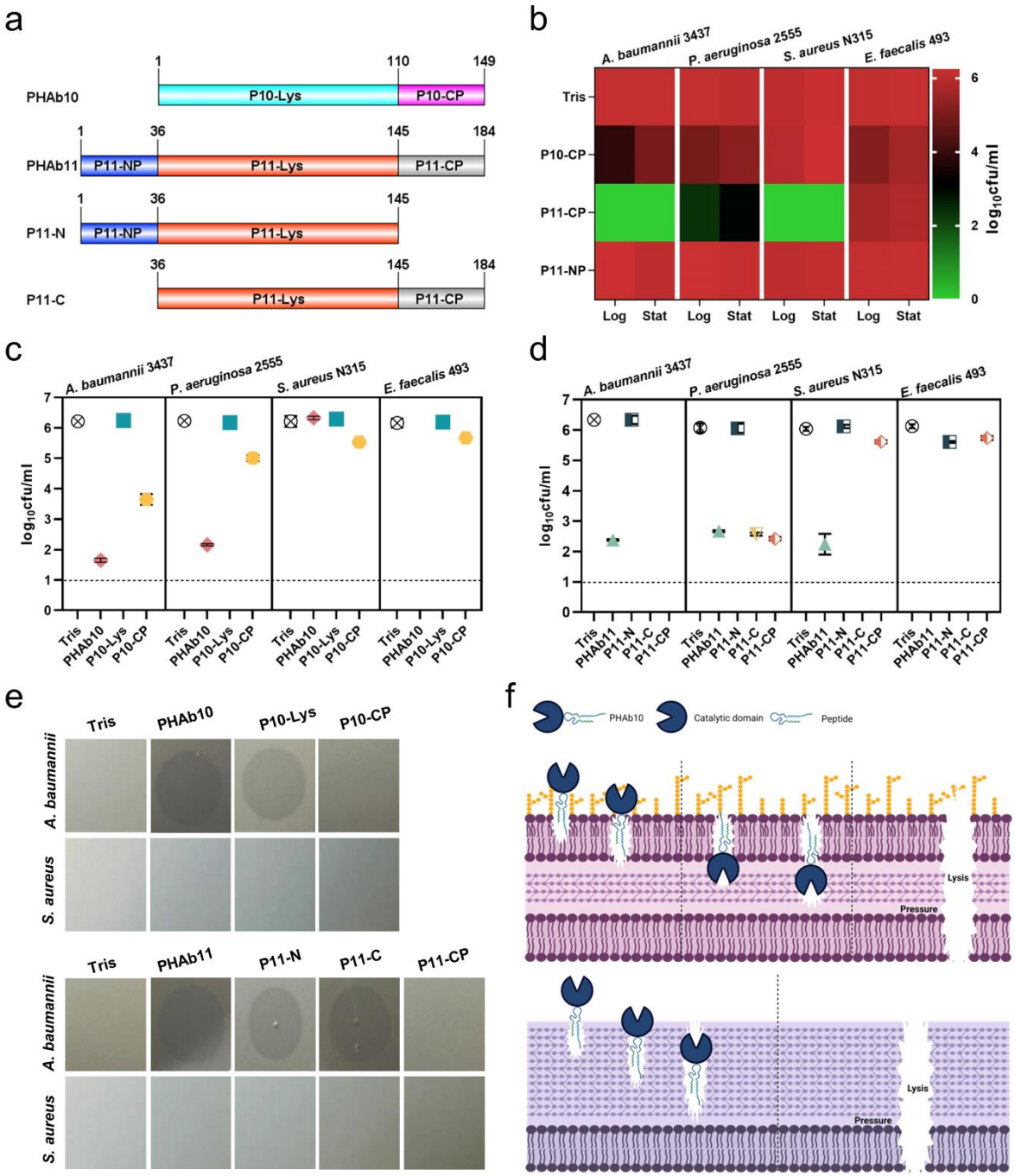

Fig. 3 Mechanism of action of PHAb10 and PHAb11 on Gram-negative and Gram-positive bacteria. (a) Schematic representation of PHAb10 and PHAb11 domains. (b) Bactericidal activity of peptides derived from PHAb10 and PHAb11. Bacterial cells are treated with 50 μg/ml P10-CP, P11-NP, or P11-CP in 20 mM Tris-HCl at 37°C for 1 hour. (c-d) Bactericidal activity of different truncations of PHAb10 and PHAb11. Exponential *A. baumannii* 3437 cells are incubated with 50 μg/ml of each truncated fragment in 20 mM Tris-HCl for 1 hour at 37°C. Dash lines represent the limit of detection and data below the limit of detection is not shown. (e) Peptidoglycan hydrolytic activity of different

297 truncations of PHAb10 and PHAb11. 0.1 μg of each truncated fragment is dropped onto autoclaved
298 lawns of *A. baumannii* 3437 and *S. aureus* N315 and incubated at 37°C for 4 h. The groups treated with
299 an equal volume of 20 mM Tris-HCl served as controls. (f) Schematic bactericidal mechanisms of
300 PHAb10 against Gram-negative and Gram-positive bacteria.
301

302 **PHAb8 is a thermosensitive monomer, whilst PHAb10 and PHAb11 formed a**
303 **thermostable dimer**

304 To understand the catalytic mechanism and thermal stability of these novel peptidoglycan
305 hydrolases, we solved the crystal structures of PHAb8, PHAb10, and PHAb11 by X-ray
306 crystallography (Table S2), and the results showed that PHAb8 was a monomer (Fig. 4a and
307 Fig. S4a), whilst PHAb10 (Fig. 4b) and PHAb11 (Fig. 4c) formed an asymmetric dimer.
308 Specifically, the two asymmetric units of PHAb10 formed an antiparallel dimer with a rotation
309 angle of 177.2° along the rotation axis and a distance of 10.5 Å between them. Further, PHAb10
310 dimer adopted a circularly permuted architecture, in which the N-terminus of one chain and the
311 C-terminus of another chain formed a cavity, which might be the binding site of the
312 peptidoglycan substrate (Fig. 4b). The two subunits of PHAb11 formed a tail-to-tail dimer with
313 a rotation angle of -179.4° along the rotation axis and a distance of 37.1 Å between them. Each
314 PHAb11 monomer contained an independent substrate-binding cavity around its catalytic triad
315 (Fig. 4c). Notably, the N-terminal 36 amino acids, P11-NP, were missing in our PHAb11 dimer.
316 We speculated that it may be destroyed during crystal formation. Interestingly, PHAb8 showed
317 high topological similarity to monomeric PHAb10 and PHAb11, with the typical catalytic triad
318 (Glu-Asp-Thr) located at the coil region (Fig. 4d and Fig. S4a-c). Dali-based screening further
319 showed that the catalytic triad of PHAb8, PHAb10, and PHAb11 were highly conserved in
320 homologous proteins, including AcLys (PDB ID 6ET6), LysF1 (PDB ID 7M5I), SpmX-Mur-
321 *Ae* (PDB ID 6H9D), P22 (PDB ID 2ANX), and R21 (PDB ID 3HDE) (Fig. S4d and Table S3).
322 Superimposition of PHAb8, PHAb10, PHAb11 with other well-known lysozymes, including
323 hen egg-white lysozyme (HEWL, PDB ID 4HPI), goose egg-white lysozyme (GEWL, PDB ID
324 153L), T4 lysozyme (T4L, PDB ID 1LYD), and lambda lytic transglycosylase (PDB ID 1LYD)
325 revealed that the overall structures of PHAb8, PHAb10, and PHAb11 had relatively low
326 similarity to HEWL, GEWL, and lambda lytic transglycosylase (Fig. S4e-g). Despite their
327 lower amino acid sequence similarity (Fig. S4h), PHAb8, PHAb10, and PHAb11 superimposed
328 well with T4 lysozyme, especially in their Glu-Asp-Thr catalytic triad regions (Fig. S4i and
329 Table S3), suggesting that PHAb8, PHAb10, and PHAb11 may be phage-originated. Supporting

330 to this, all three enzymes were predicted to be originated from prophages by PhageBoost (Fig.
331 S5). All these observations together indicated that PHAb8, PHAb10, and PHAb11 were highly
332 evolutionarily related to T4 lysozyme and might share similar catalytic mechanisms of action.
333
334 To reveal which domain contributes to the thermal stability of PHAb10 and PHAb11, we
335 examined the residual bactericidal activity of their individual domains by treating them at
336 100°C for 1 hour. Results showed that for all strains tested, the holoenzyme and its antimicrobial
337 peptide domain P10-CP retained high bactericidal activity, but its lysozyme catalytic domain
338 P10-Lys did not (Fig. 4e). Except for the N-terminal peptide P11-NP, other truncated PHAb11
339 still maintained substantial bactericidal activity after heating at 100°C for 1 hour (Fig. 4f). These
340 observations raised the question of whether PHAb10 and PHAb11 dimers are hyper-
341 thermostable. To test this, we determined the temperature-dependent denaturation of these
342 enzymes by nano-differential scanning fluorimetry (nanoDSF). Our results showed that PHAb8,
343 PHAb10, and PHAb11 were denatured with transition temperatures of 41.4, 53.7, and 59.9°C,
344 respectively (Fig. 4g). Interestingly, signs of aggregation were only observed in PHAb8 but not
345 in PHAb10 and PHAb11 (Fig. S4j), indicating that PHAb10 and PHAb11 underwent structural
346 refolding without precipitation during heat treatment. Consistent with these observations, the
347 corresponding circular dichroism (CD) curves of PHAb8, PHAb10, and PHAb11 at 90°C were
348 significantly different from their corresponding curves at temperature close to their transition
349 temperature (Fig. 4h-j), suggesting that, similar to PHAb8, PHAb10 and PHAb11 lost their
350 native conformation at high temperature such as 90°C. To further understand the
351 thermodynamics of PHAb10 and PHAb11, we examined the structure of PHAb10 before and
352 after heat treatment at 100°C for 1 hour by CD. Intriguingly, only minor differences were
353 observed before and after heat treatment (Fig. 4k), indicating that PHAb10 almost refolded to
354 its native conformation during cooling after heat treatment. The C-terminal antimicrobial
355 peptide P10-CP of PHAb10 could withstand heat treatment, but P10-Lys was deformed after
356 being treated at 100°C for 1 hour (Fig. 4l). Similar to the folding-refolding phenomenon of
357 PHAb10, PHAb11 and its N-terminal peptide-deleted variant P11-C could restore to their native
358 conformation after 1 hour treatment at 100°C (Fig. 4m-n), whilst its C-terminal peptide-deleted
359 variant P11-N could not refold to its native conformation (Fig. 4o), indicating that C-terminal
360 peptide was essential for its hyper-thermostability. Altogether, these observations suggested that
361 dimerized PHAb10 and PHAb11 possessed unique folding-refolding thermodynamic
362 mechanism.

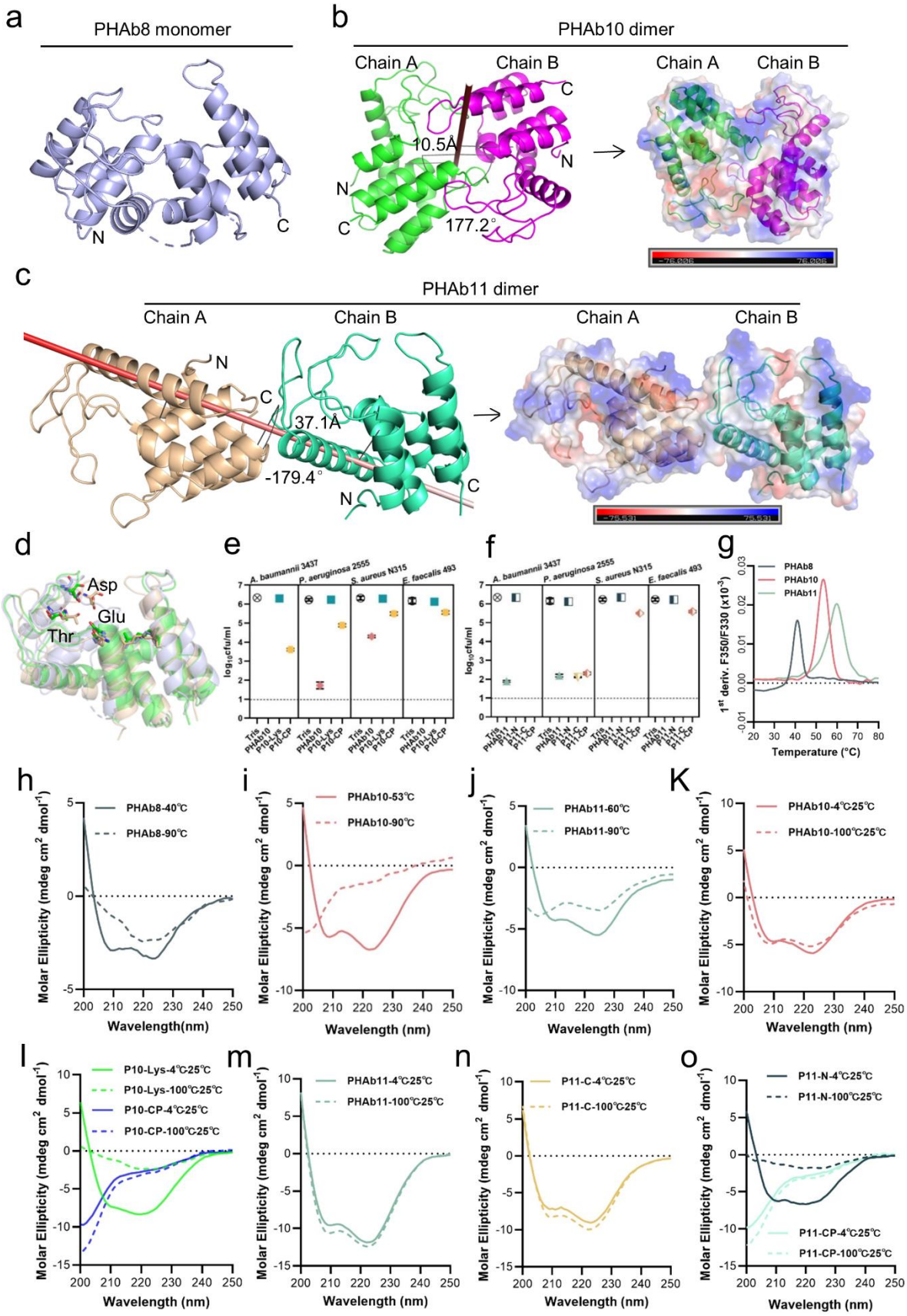

Fig. 4 PHAb10 and PHAb11 are thermostable dimers. (a) Overall structure of PHAb8 monomer. (b) Dimeric structure of PHAb10. Chain A is colored in green, Chain B is colored in magenta, and the gray stick

366 denotes the rotation axis. The electrostatic surface of PHAb10 with two potential substrate binding cavities
367 are shown (negative = red; positive = blue). (c) Dimeric structure of PHAb11. Chain A is colored in wheat,
368 Chain B is colored in green-cyan, and the red stick denotes the rotation axis. The electrostatic surface of
369 PHAb11 with two potential substrate binding cavities is also shown (negative = red; positive = blue). (d)
370 Superimposition of monomeric PHAb8, PHAb10, and PHAb11. PHAb8 is shown in light blue, PHAb10 in
371 green, and PHAb11 in wheat. Residues involved in the catalytic triad are shown in sticks. (e-f) Residual
372 bactericidal activity of PHAb10, PHAb11, and their truncation variants. Each truncation variant is treated at
373 100°C for 1 hour, stored at 25°C for 1 hour, and then tested for bactericidal activity by a log-killing assay.
374 Dash lines represent the limit of detection and data below the limit of detection is not shown. (g) Thermal
375 unfolding curves of PHAb8, PHAb10, and PHAb11 from 20 to 100°C as determined by nanoDSF. Values
376 on the y-axis represent the first derivative of the fluorescence ratio at 350 nm and 330 nm. Peaks represent
377 the transition temperature of each protein. (h-j) Circular dichroism spectra of PHAb8 (h), PHAb10 (i), and
378 PHAb11 (j) at 90°C and temperatures close to their transition temperatures. (k-o) Circular dichroism spectra
379 of PHAb10, PHAb11, and their truncation variants before and after heat treatment. Each domain fragment is
380 treated at 100°C for 1 hour, stored at 25°C for additional hour prior to CD detection.

381

382 **Folding-refolding thermodynamic of PHAb10 dimer is governed by intermolecular**
383 **interactions**

384 Since PHAb10 dimer and PHAb11 dimer exhibit a similar folding-refolding thermodynamic
385 profiles, we wondered whether it was achieved through dimer-monomer switching. Therefore,
386 we used PHAb10 as an example to test this hypothesis. We carefully examined the topology of
387 the PHAb10 dimer and found that it was supported by 7 pairs of intermolecular H-bonds, with
388 3 pairs supporting the head, each 2 pairs in midbody and tail of the PHAb10 dimer (Table S4).
389 Specifically, in the top view of chain A, Arg20 and Gly27 were involved in intermolecular H-
390 bond interactions, supporting the head region, Gly128 and Gly129-mediated interaction
391 contributed to the stability of midbody, whilst Lys133 and Arg137 were involved in
392 intermolecular H-bond forces anchoring the tails of the PHAb10 dimer (Fig. 5a and Table S4).
393 Next, we constructed several PHAb10 variants involving depletion of intermolecular force at
394 the head, midbody, tail, or entire entity of the PHAb10 dimer (Table S5). Since PHAb10 was a
395 verified dimer after chemical cross-linking in SDS-PAGE gel (Fig. 5b), we further examined
396 the polymerization of these PHAb10 variants by Native-PAGE. As shown in Fig. 5c, wildtype
397 PHAb10 showed two bands corresponding to its monomeric and dimeric forms. Whilst the
398 variants R20IG27D, which has mutations in the head-supporting site, and G27DR137I, which

399 has mutations in both the head and tail supporting sites, lost dimerization ability. As a result,
400 both variants lost most of their bactericidal activity after treatment at 100°C for 1 hour (Fig.
401 5d), which could be further explained by the failure to recover their native forms after heat
402 treatment (Fig. 5e-f). In support of these observations, the variant PHAb10-mut containing
403 mutations in all 7 pairs of dimer-supporting sites showed aborted bactericidal activity (Fig. 5d)
404 and failed to recover its native conformation (Fig. 5e-f) after treatment at 100°C for 1 hour. In
405 contrast, the variants G128D/G129D with mutations in the midbody-supporting sites still
406 showed a mixture of monomers and dimers (Fig. 5c), indicating that depletion of the midbody-
407 supporting force hardly affected the dimerization of PHAb10. Consistent with this observation,
408 the variant G128D/G129D still remained intact bactericidal activity (Fig. 5d) and could refold
409 to its native form after heat treatment (Fig. 5e-f). Moreover, the variant K133A/R137I with
410 mutations in the tail-supporting site also showed aborted bactericidal activity (Fig. 5d) and an
411 irreversible conformation change after heat treatment (Fig. 5e-f), although it maintained a weak
412 dimerization ability (Fig. 5c). This suggested that intermolecular forces at the tail of the
413 PHAb10 dimer had only a small impact on its thermodynamics properties. Taken all these
414 observations together, we proposed a model by which the PHAb10 dimer executed its folding-
415 refolding thermodynamics (Fig. 5g). At temperatures above its transition point (i.e., >53.7°C),
416 dimerized PHAb10 dissociated into monomers without precipitation. During the cooling
417 process, monomeric PHAb10 refolded to a stable dimer *via* the intermolecular interactions
418 between the two monomers, i.e., three pairs of intermolecular bonds at the head, two in the
419 midbody, and two at the tail of the PHAb10 dimer. The folding and refolding dynamics of
420 PHAb10 after heat treatment were somewhat similar to the opening and closing of zippers,
421 where the intermolecular bonds act as inducers.

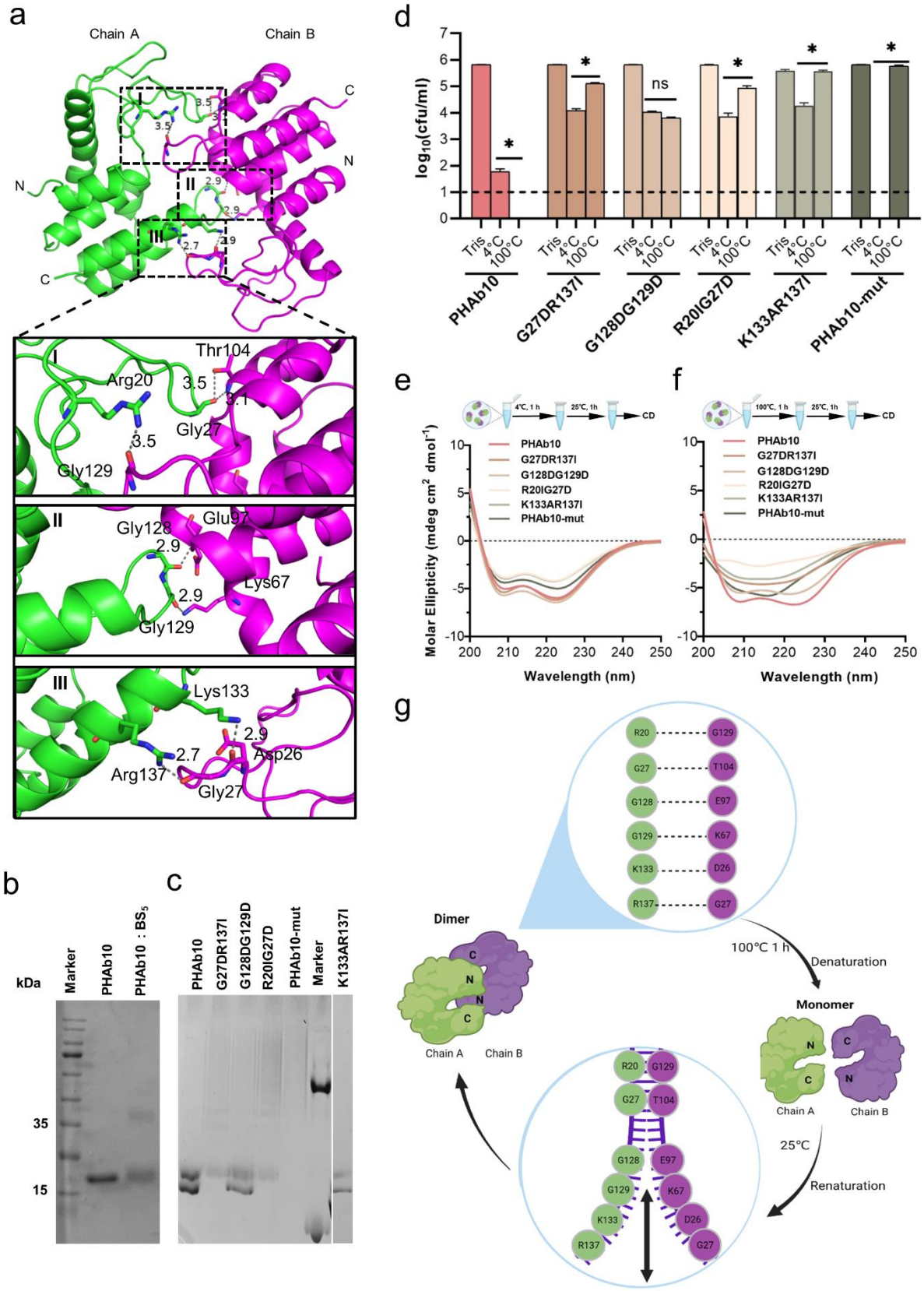

Fig. 5 Folding-refolding thermodynamics of PHAb10. (a) Intermolecular interactions of PHAb10 dimer. The residues involved are shown as sticks. (b) SDS-PAGE analysis of PHAb10 with or without chemical cross-linker. (c) Native-PAGE analysis of PHAb10 and its variants. Marker: the upper band represents BSA

426 (66.4 kDa), and the lower band represents lysozyme (14 kDa). (d) Bactericidal activity of PHAb10 and its
427 variants before and after heat treatment. Each protein is incubated for 1 hour at 4 or 100°C, stored at 25°C
428 for an additional 1 hour, and then examined for bactericidal activity in 20 mM Tris-HCl (pH 7.4) at a
429 concentration of 50 μg/ml against exponential *A. baumannii* 3437 cells for 1 hour. Dash lines represent the
430 limit of detection and data below the limit of detection is not shown. Data are analyzed by two-tailed
431 Student's t-tests. ns: statistically not significant; *: $p<0.05$. (e-f) Circular dichroism spectra of PHAb10 and
432 its mutants before and after treatment at 100°C for 1 hour. (g) Zipper model showing the thermodynamics of
433 PHAb10 dimer.

434

435 **PHAb10 efficiently removes *A. baumannii* from infection sites *in vivo***

436 Since PHAb10 showed rare cytotoxicity on cell level (Fig. S6), we further tested its bactericidal
437 activity in two different mouse infection models. In the burn wound model of *A. baumannii*
438 infection (Fig. 6a), mice were first treated with 10 μg/mouse PHAb10 (10 μl; n = 5) for 4 hours,
439 and then infected with 10 μl 5×10^8 cfu/ml of *A. baumannii* 3437 for 24 hours. We found
440 significantly less viable bacteria remaining at the site of infection compared to Tris-treated
441 controls (Fig. 6b). Treatment with 4 μg/mouse minocycline (10 μl; n = 5) also showed good
442 bacterial removal compared to the control group, however, no statistical difference was
443 observed between groups treated with 10 μg/mouse PHAb10 and 4 μg/mouse minocycline (Fig.
444 6b), suggesting that when administered topically, PHAb10 was as efficient as minocycline in
445 clearing susceptible bacteria from the site of infection. In the mouse abscess model, mice were
446 infected hypodermically (i.h.) with 25 μl of *A. baumannii* 3437 at a concentration of 5×10^8
447 cfu/ml for 24 hour, and then treated with 10 μg/mouse PHAb10 (10 μl; n = 6) or 4 μg/mouse
448 minocycline (10 μl; n = 7) subcutaneously for 5 days. Six days after infection, viable bacteria
449 were recovered from the infection site and counted (Fig. 6c). Our results showed that there was
450 rare difference between the minocycline-treated group and the Tris-treated control group (Fig.
451 6d). In contrast, a significant reduction in residual *A. baumannii* was observed in the PHAb10-
452 treated group (Fig. 6d), indicating that PHAb10 had better bactericidal efficacy than
453 minocycline when injected subcutaneously at the site of infection in a skin infection model.
454 Notably, rare differences were observed in changes in animal body weight from groups treated
455 with either PHAb10, minocycline, or Tris buffer (Fig. 6e). Taking all these observations

456 together, PHAb10 appeared to exhibit good bacterial clearance efficacy *in vivo* and might
457 represent a novel antimicrobial agent for the treatment of drug-resistant bacteria.

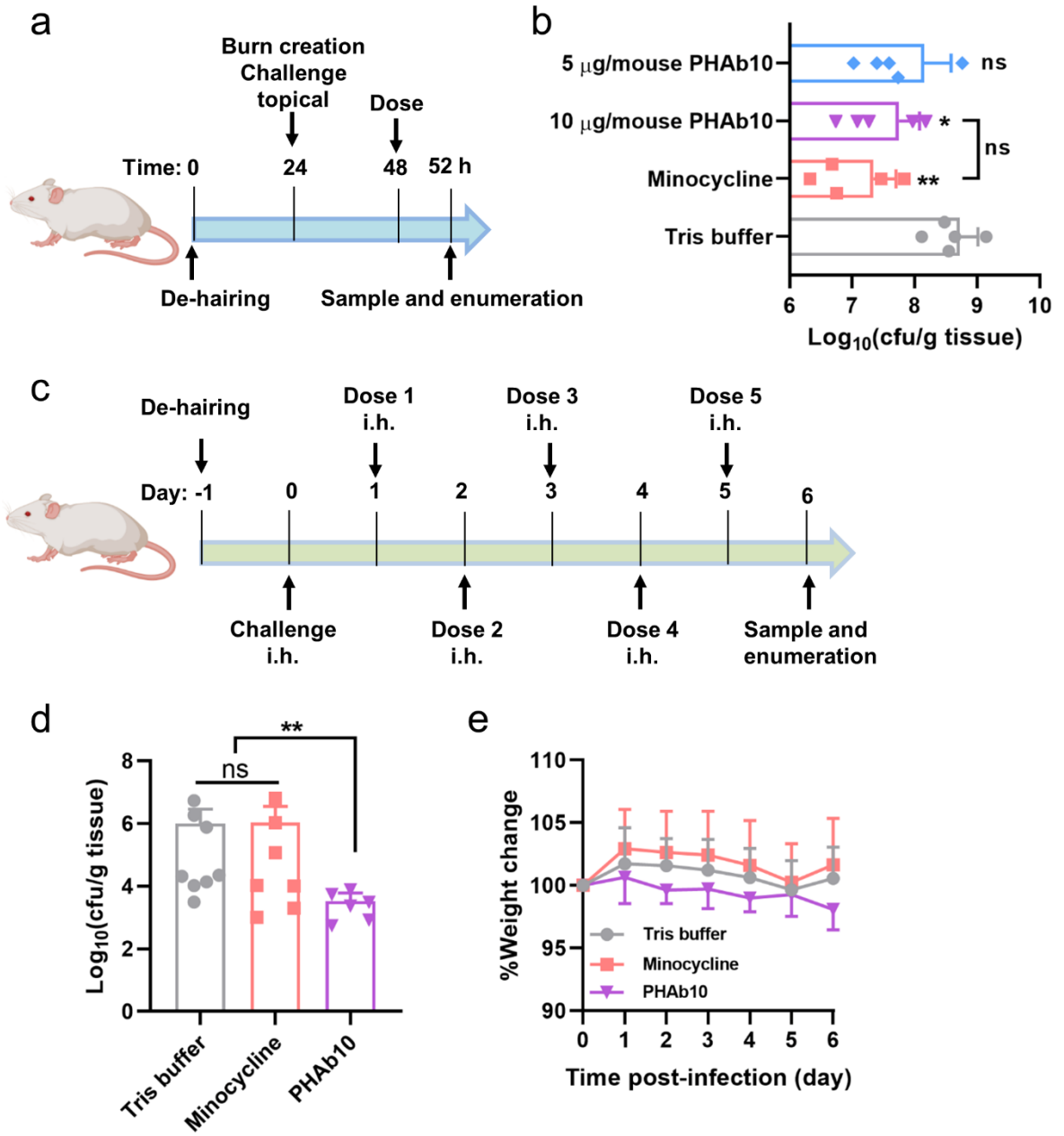

458

459 **Fig. 6 PHAb10 shows high efficacy in mouse infection models.** (a) Experimental schema for burn wound
460 infection model. Burn wounds produced by exposing naked skin to 65°C water for 12 s was infected with 10
461 μl 5×10^8 cfu/ml of *A. baumannii* 3437. At 24-hour post-colonization, mice are treated with 5 or 10
462 μg/mouse PHAb10 (10 μl; n = 5), 4 μg/mouse minocycline (10 μl; n = 5), or an equal volume of Tris
463 buffer (10 μl; n = 5). Four hours post-treatment, viable bacteria on the burn wound skin is collected and
464 counted. (b) Viable *A. baumannii* collected from burn wound skin after each treatment. The number of

465 viable cells in each group is normalized and compared with the number of viable cells treated with Tris
466 buffer by ANOVA. ns: statistically not significant; *: $p<0.05$; **: $p<0.01$. (c) Experimental schema for
467 abscess model. Mice are infected hypodermically with 25 μl 5×10^8 cfu/ml of *A. baumannii* 3437 on the
468 right side of the back dorsum. Twenty-four hours after infection, mice are injected hypodermically with
469 10 μg/mouse PHAb10 (10 μl; n = 6), 4 μg/mouse minocycline (10 μl; n = 7), or an equal volume of Tris
470 buffer (10 μl; n = 8). Each group is injected subcutaneously once a day for 5 consecutive days. Viable
471 bacteria in site of infection are counted 24 hour after the last dose. (d) Viable *A. baumannii* collected
472 from skin after each treatment. The number of viable cells from each group is normalized and compared
473 with the number of viable cells treated by the Tris buffer by ANOVA. ns: statistically not significant; **:
474 $p<0.01$. (e) Changes in mice body weight per treatment group.
475

476 **Discussion**

477 The uncontrollable spread and emergence of antimicrobial resistance requires the discovery of
478 novel antimicrobial agents with different targets or mechanisms of action from traditional
479 antibiotics. Policy makers, scientists, enterprisers, and investigators have worked together for
480 decades to exploit the 'trojan horse' globally, but new options for treating antimicrobial
481 resistance in the clinic remain to be seen. Bacteriophage-derived peptidoglycan hydrolases (i.e.,
482 lysins) have been considered as promising alternatives against drug-resistant bacteria due to
483 their potent bactericidal activity, low risks of drug resistance, and unique mechanism of action,
484 as witnessed by several ongoing clinical trials targeting on Gram-positive bacteria. However,
485 for Gram-negative bacteria, the effects of phage-derived lysins were often hampered by their
486 outer membranes, which requires more strategies to overcome. In the present work, we report
487 a new strategy to mine novel bactericidal peptidoglycan hydrolases from bacterial proteomes
488 through lysin-derived antimicrobial peptide-priming screening. As a proof-of-concept, we
489 successfully discovered two novel peptidoglycan hydrolases from the *A. baumannii* proteome
490 using PlyF307 lysin-derived peptide as a template, highlighting the utility of this strategy in
491 mining antimicrobial agents from bacterial database.

492 Notably, PHAb10 and PHAb11 exhibited high bactericidal activity against a variety of Gram-
493 negative and Gram-positive microbes. Unlike other Gram-negative lysins that act in an outer
494 membrane permeabilizer-dependent manner (41-44), PHAb10 and PHAb11 exhibited intrinsic

activity against Gram-negative and Gram-positive pathogens *via* different mechanisms of action. Due to their C-terminal antimicrobial peptides, namely, P10-CP and P11-CP, PHAb10 and PHAb11 were able to penetrate the outer membrane of Gram-negative bacteria in an auto-priming manner, allowing them to access and cleave peptidoglycan bonds, ultimately leading to osmotic lysis of Gram-negative pathogens. For Gram-positive bacteria, they are primarily killed through the action of intrinsic antimicrobial peptides. Interestingly, we noted a difference in the killing of Gram-positive bacteria by PHAb10 and PHAb11, which may be due to the fact that P11-CP had one more basic amino acid than P10-CP, so it had stronger bactericidal activity. In addition, compared to other naturally occurring lysins such as PlyPa03, PlyPa91, and PlyE146 (37, 45), PHAb10 and PHAb11 showed traceable bactericidal activity even at concentrations as low as 0.625 μg/ml.

Structure-based homology analysis revealed that PHAb10 and PHAb11 probably belonged to the T4 lysozyme family and possessed the conserved Glu-Asp-Thr catalytic triad shared by traditional phage lysins and bacterial autolysins, namely Glu17, Asp26, and Thr32 of PHAb10, and Glu52, Asp61, and Thr67 of PHAb11. However, unlike most other enzymes reported to date, PHAb10 and PHAb11 exhibited excellent thermostability, retaining almost 100% bactericidal activity after treatment at 100°C for 1 hour. In contrast, gp36C lysin from bacteriophage ϕKMV, a known highly thermostable lysozyme, retains only ~50% residual activity after 1 hour of treatment at 100°C (46, 47). Also, T4 lysozyme derived from T4 phage, which shares 44% sequence similarity and 27% sequence identity with gp36C, was completely inactivated after treatment at 75°C for 5 minutes (48). To the best of our knowledge, phage-derived lysins with such high thermostability similar to PHAb10 and PHAb11 had yet to be described. Heat-resistant lysin have potential applications in animal feed premixes (pelletizing temperature 75-98°C) and medical devices requiring autoclaving.

To the best of our knowledge, few proteins have been demonstrated to have reversible folding-refolding thermodynamics at high temperature, but their mechanisms are unclear, such as HPL118, HPL511, and HPLP35 (49). Here we found that PHAb10 had a unique temperature-dependent folding-refolding thermodynamic, and structural and biochemical analyses further suggested that PHAb10 undergoes a unique dimer-monomer switching mediated by 6 pairs of intermolecular interactions to survive heat treatment. To our knowledge, this is the first time

525 that an enzyme had been found to adapt to ambient temperature by altering its dimerization
526 state.
527 Bacteriophages are known to be the most abundant biological entities on earth (50). Over
528 billions of years of coevolution, more than 80% of bacterial genomes have become populated
529 with at least one prophage (51, 52), also known as molecular imprints, which serve as an
530 untapped arsenal for the discovery of phage-related antimicrobial agents. Notably, prophage
531 identification lags greatly behind genome or metagenome sequencing. Therefore, there is
532 reason to believe that advances in bacterial culturomics (53), 'rebooting' phage genomes in
533 more tractable hosts (54), and computational biology (55, 56), may help discover otherwise
534 inaccessible prophages from bacterial genome big data. In turn, this will increase the added
535 value of bacterial genome as a new source of unearthed therapeutically promising antimicrobial
536 drugs. More importantly, our findings implied that daily updated big data, such as bacterial
537 genomes and proteomes, human proteomes, and various metagenomic data, could in principle
538 became an encrypted power in the fight against antimicrobial resistance.
539

540 **Materials and Methods**

541 **Bacterial strains**

542 The bacterial strains used in this work are described in Table S6. *Acinetobacter baumannii*,
543 *Escherichia coli*, *Pseudomonas aeruginosa*, *Klebsiella pneumoniae*, *Enterococcus faecalis,* and
544 *Staphylococcus aureus* were all grown in Lysogeny Broth (LB) at 37°C. *Streptococcus*
545 *pneumoniae* was stationary cultured in Todd Hewitt Broth with 0.5% Yeast extract (THY) at
546 37°C with 5% CO_2. All other *Streptococci* were grown in Brain Heart Infusion (BHI) broth at
547 37°C.

548 **Screening of putative peptidoglycan hydrolases from *A. baumannii***

549 Putative peptidoglycan hydrolases from the *A. baumannii* (PHAbs) proteome database were
550 obtained by BLASTP in NCBI using the lysin PlyF307-derived antimicrobial peptide P307 as
551 input sequence. Sequences marked as partial, shorter than 110 amino acids, longer than 300
552 amino acids, or clearly not belonging to lysins were manually excluded from further analysis.
553 Multiple sequence alignments were performed by the ClustalW algorithm in MEGAX software
554 and visualized by Jalview. Phylogenetic tree was further constructed by MEGAX software

555 using the Neighbor-Joining method and visualized by the iTOL online service
556 (http://itol.embl.de/). Three-dimensional (3D) protein models showing different amino acid
557 residues were predicted online by SWISS-MODEL (https://swissmodel.expasy.org/).

558 ***In silico* analysis of PHAbs**

559 The basic physical and chemical properties of PHAbs were analyzed by ProtParam
560 (https://web.expasy.org/protparam/). Solubility was predicted by Protein-Sol (https://protein-
561 sol.manchester.ac.uk/), and signal peptides were predicted by SignalP
562 (https://services.healthtech.dtu.dk/service.php?SignalP-5.0). The transmembrane area was
563 predicted by TMHMM (https://services.healthtech.dtu.dk/service.php?TMHMM-2.0), while
564 domain predictions were performed through CD searches in the NCBI database
565 (https://www.ncbi.nlm.nih.gov/Structure/cdd/wrpsb.cgi) and InterPro in the EBI database
566 (http://www.ebi. ac.uk/interpro/search/sequence/). The Percent Identity Matrix was calculated
567 by Clustal Omega (https://www.ebi.ac.uk/Tools/msa/clustalo/) and visualized with TBtools.
568 The prophage origination analysis was predicted by PhageBoost (https://phageboost.ku.dk/)
569 (57). The net charge of the N-terminal and C-terminal 30 amino acids of each PHAb was
570 calculated by BaAMPs (http://www.baamps.it/tools/calculator) under neutral condition. The
571 Local Net Charge of each PHAb was obtained by assigning 1 to the basic amino acids Arg (R)
572 and Lys (K) and -1 to the acidic amino acids Glu (E) and Asp (D) and summing all assignments
573 in a 31 amino acid window composing of 15 amino acids before and after the determined
574 position. The 3D models of each PHAb were predicted by AlphaFold2 and visualized by
575 PyMOL.

576 **Gene synthesis and cloning**

577 The coding sequences of the original five putative peptidoglycan hydrolases, namely, PHAb7,
578 PHAb8, PHAb9, PHAb10, and PHAb11, as well as the PHAb10 variant, PHAb10-mut with 6
579 site mutations were chemically synthesized with codon optimization and cloned into *Nco*I and
580 *Xho*I restriction sites of the pET28b(+) vector. Additional variants of PHAb10 and truncations
581 of PHAb10 and PHAb11 were constructed by primer-derived overlap PCR (Table S7). All
582 constructs were electro-transformed into *E. coli* BL21(DE3) competent cells for expression.
583 Peptides derived from PHAb10 and PHAb11, namely P10-CP (amino acids 111-149), P11-NP
584 (amino acids 1-36), and P11-CP (amino acids 146-184), were chemically synthesized and

585 dissolved in ultrapure water before use.

586 **Protein purification**

587 BL21(DE3) cells were grown in LB to an optical density at 600 nm (OD_{600}) of 0.4-0.6 and
588 induced with 0.2 mM isopropyl β-D-thiogalactopyranoside at 37°C for 2 h. Cells were then
589 harvested and lysed by sonication. Supernatant was collected and passed through a Ni-NTA
590 column pre-equilibrated with 20 mM imidazole. Fractions were collected by washing and
591 eluting with 60 mM and 250 mM imidazole, respectively. The collected active protein fractions
592 were pooled, dialyzed against 20 mM Tris-HCl (pH 7.4), and then filter-sterilized. Protein for
593 crystallization was further purified by size-exclusion chromatography on a Superdex 75 (GE
594 Healthcare) with gel filtration buffer (50 mM Tris-HCl, pH 8.0, 150 mM NaCl, 1 mM DTT).
595 Protein purity was examined by 12% SDS-PAGE, and protein concentration determined using
596 the BCA Protein Concentration Assay Kit. Dimerization of PHAb10 and its variants was
597 detected by Native-PAGE.

598 **Halo assay**

599 Bacterial strains were grown overnight in 100 ml LB, harvested, and resuspended in 50 ml
600 phosphate buffered saline (PBS) containing 0.7% agarose. Cells were then autoclaved and
601 poured into glass Petri dish culture plates. Ten microliter of peptidoglycan hydrolases at
602 different concentrations (0, 2.5, 5, and 10 μg/ml) were dropped onto each bacterial lawn and
603 incubated at 37°C till a clear zone was formed, and its area was determined using the method
604 previously described (58). Wells treated with an equal volume of 20 mM Tris-HCl were used
605 as controls.

606 **Antibacterial activity assay**

607 To determine the antibacterial activity of peptidoglycan hydrolases, bacteria were cultured
608 overnight (stationary phase, OD_{600} = 1.2-1.6), then transferred to fresh medium at 100-fold
609 dilution and continued to grow for 3 hours to OD_{600} = 0.5-0.6 in the exponential growth phase.
610 Cultures of different bacteria were centrifuged at 10,000 × *g* for 1 minute, washed once and
611 resuspended in 20 mM Tris-HCl, pH 7.4. Stationary phase bacterial cells were diluted to a final
612 OD_{600} of 0.6 before use. To test the bactericidal activity of each peptidoglycan hydrolase, 100
613 μl of a bacterial suspension in stationary phase or exponential phase was mixed with an equal
614 volume of peptidoglycan hydrolase at different concentrations at 37°C for 1 hour with shaking

615 at 200 rpm. The number of viable bacteria after each treatment was counted by plating serial
616 dilutions on LB agar. Wells treated with an equal volume of dialysis buffer instead of
617 peptidoglycan hydrolases were used as controls. Specifically, to test the dose-dependent
618 antibacterial activity of PHAb10 and PHAb11, exponential cultures of various Gram-negative
619 and Gram-positive bacteria were treated with 0, 0.625, 1.25. 2.5, 5, 6.25, 10, 12.5, 25, 50, or
620 100 μg/ml of each enzyme in 20 mM Tris-HCl (pH 7.4) at 37°C for 1 hour.
621 To test the time-killing curves of PHAb10 and PHAb11 against exponential *A. baumannii* 3437,
622 bacterial suspensions were incubated with 50 μg/ml of each peptidoglycan hydrolase in 20 mM
623 Tris-HCl (pH 7.4) for 0, 0.5, 1, 3, 5, 10, 15, 30 ,45, 60, and 120 min at 37°C.
624 To measure the effects of different environmental factors on the antibacterial activity of
625 PHAb10 and PHAb11, exponential *A. baumannii* 3437 cells were treated with 50 μg/ml of each
626 peptidoglycan hydrolase at different pH values (5, 6, 7, 8, 9, and 10), various temperatures (4,
627 25, 37, 45, 55, 65, 75, 85, and 100°C), and various NaCl concentrations (0, 25, 50, 100, 200,
628 500, and 1000 mM), and urea (0, 50, 100, 200, 500, and 1000 mM) at 37°C for 1 hour. All
629 assays were performed at least three times in biological replicates.
630 **Thermostability assay**
631 The thermostability of PHAb and their variants at 100 μg/ml was determined by a Prometheus
632 NT.48 nano-differential scanning fluorimetry (nanoDSF, NanoTemper Technologies, CA, USA)
633 in the temperature range of 20-100°C (increasing step of 1°C/min) in 20 mM Tris-HCl (pH 7.4).
634 The first derivative of the fluorescence ratio at 350 and 330 nm (1st der, F350/F330) was
635 calculated automatically by the PR-ThermControl software supplied with the instrumentation.
636 The transition temperature (Tm) corresponds to the 1st order peak of F350/F330.
637 **Circular dichroism**
638 The circular dichroism spectra of PHAb and its variants at 200 μg/ml in 20 mM Tris-HCl (pH
639 7.4) were collected by an Applied Photophysics Chirascan Plus circular dichroism spectrometer
640 (Leatherhead, UK) from 200-260 nm (0.1 cm path length) at room temperature. The spectra of
641 air and Tris-HCl buffer (pH 7.4) were recorded as background and baseline, respectively.
642 Secondary structures were calculated by CDNN V2.1 software supplied by the instrument
643 manufacturer.
644 **Crystallization, data collection and processing.**

645 In this study, crystals were obtained for each protein at a concentration of 20-25 mg/ml using
646 sitting drop method at a 1:1 ratio on a reservoir of 0.1 M citric acid pH 3.5, 25% w/v
647 polyethylene glycol 3350 after 1 week of incubation at 16°C. They were then immersed in a
648 cryoprotectant consisting of a reservoir solution supplemented with 10% glycerol before being
649 flash frozen in liquid nitrogen. Diffraction data were collected at beamline 19U1 (BL19U1) at
650 Shanghai Synchrotron Radiation Facility (SSRF), and the X-ray datasets were processed using
651 HKL2000 and XDS software programs. The initial phase information was determined by
652 molecular replacement in the program PHASER using *A. baumannii* AB 5075UW prophage
653 (PDB code: 6ET6) as the initial search model. The structure was then improved by multiple
654 rounds of manual construction and refinement by COOT and PHENIX. The final structures of
655 PHAb8, PHAb10, and PHAb11 were visualized using PyMOL and deposited in the PDB
656 database with access numbers 8HEM, 7YKU, and 8HDQ, respectively. Summary of data
657 collection and refinement statistics are presented in Table S2.

658 **Cytotoxicity testing.**

659 The cytotoxicity of PHAb10 against HepG2 cells was determined by a Cell Counting Kit-8
660 (CCK-8) assay (Dojindo Molecular Technologies, Kumamoto, Japan) according to the
661 manufacturer's protocol. HepG2 cells were seeded in 96-well plates at a density of 5,000 cells
662 per well in Dulbecco's modified Eagle medium (DMEM; Sigma-Aldrich, Shanghai, China)
663 supplemented with 10% fetal bovine serum, 1% penicillin, and 1% streptomycin for 24 h. The
664 cells were then exposed to a series of concentrations of PHAb10 (0, 6.25, 12.5, 25, 50, and 100
665 μg/ml) for another 24 h. Afterwards, the contents of the plates were replaced with fresh medium
666 containing 10% CCK-8 solution and incubated at 37°C for 1.5 h. The final optical density at
667 OD450 was noted by use of a microplate reader (SynergyH1; BioTek, USA). The results were
668 expressed as relative cell viability, expressed as a percentage of the growth of cells in control
669 wells treated with PBS only.

670 **Mouse experiments**

671 All mouse infection experiments were conducted in an ABSL-2 lab, and all experimental
672 methods were carried out in accordance with the regulations and guidelines set forth by the
673 Animal Experiments Committee of the Wuhan Institute of Virology, Chinese Academy of
674 Sciences. All experimental protocols were approved by the Animal Experiments Committee of

675 Wuhan Institute of Virology, Chinese Academy of Sciences (WIVA17202102). Animals were
676 housed in individually ventilated cages following a set of animal welfare and ethical criteria
677 during the experiment and were euthanized at the end of the observation. In the burn infection
678 model, 6- to 8-week-old female BALB/c mice were anesthetized, shaved, and depilated to
679 create a 2-cm^2 hairless area on the dorsum as previously described (35). Partial thickness burn
680 was achieved by exposing bare skin to water at 65°C for 12 s. The burns were then inoculated
681 with 10 μl 5×10^8 cfu/ml of *A. baumannii* 3437. 24 hours after colonization, mice were randomly
682 separated into four groups and treated with 5 or 10 μg/mouse PHAb10 (10 μl; n = 5), 4
683 μg/mouse minocycline (10 μl; n = 5), or an equal volume of Tris buffer (10 μl; n = 5). Four
684 hours after treatment, mice were sacrificed by cervical dislocation to obtain skin. Specifically,
685 the infected skin was excised, infiltrated in 1ml PBST (PBS containing 0.1% Triton X-100) for
686 2 min, and homogenized using a NewZongKe MD1000 Tissue Cell-Destroyer (NewZongKe,
687 Wuhan, Hubei, China). The resulting solution was serially diluted and plated on LB agar
688 containing 4 μg/ml gentamicin and 2 μg/ml meropenem. Viable cell numbers in each group
689 were analyzed by one-way analysis of variance (ANOVA).
690 In the mouse abscess model, 6- to 8-week-old female mice were depilated to create a 2-cm^2
691 hairless area on the dorsum as described above and infected hypodermically (i.h.) with 25 μl of
692 *A. baumannii* 3437 at a concentration of 5×10^8 cfu/ml on the right side of the back dorsum.
693 After 24 h of infection, mice were randomly divided into 3 groups and hypodermically treated
694 with 10 μg/mouse PHAb10 (10 μl; n = 6), 4 μg/mouse minocycline (10 μl; n = 7), or an equal
695 volume of Tris buffer (10 μl; n = 8). Subcutaneous dosage was performed once a day for 5
696 consecutive days for each group. The body weight of mice in each group was monitored daily.
697 Twenty-four hours after the last dosage, mice were sacrificed by cervical dislocation. Infected
698 skin was excised, infiltrated in 1ml PBST for 2 min, and subjected to tissue homogenization
699 using a NewZongKe MD1000 Tissue Cell-Destroyer. The resulting solution was serially diluted
700 and plated on LB agar containing 4 μg/ml gentamicin and 2 μg/ml meropenem. The number of
701 viable bacteria in each group was analyzed by ANOVA.
702

703 **Acknowledgments**

704 This work was supported by the National Natural Science Foundation of China (No. 32070187,

32161133003, 31770192, and 81802001), and the Open Research Fund Program of National Bio-Safety Laboratory, Wuhan (No. 2021SPCAS001). We thank the staff of BL19U1 beamline at National Center for Protein Sciences Shanghai and Shanghai Synchrotron Radiation Facility (Shanghai, China) for assistance during data collection. We thank Dr. Xuefang An, and Dr. Yanfeng Yao from the Core Facility and Technical Support, Wuhan Institute of Virology for their assistance in animal experiments.

Author contributions:

Li Zhang: Investigation; Methodology; Writing—review and editing. **Fen Hu**: Investigation; Methodology; Funding acquisition; Writing—original draft; Writing—review and editing. **Zirong Zhao**: Investigation; Methodology; Writing—review and editing. **Xinfeng Li**: Investigation; Methodology; Writing—review and editing. **Mingyue Zhong**: Investigation; Methodology; Writing—review and editing. **Jiajun He**: Investigation; Methodology, Writing—review and editing. **Fangfang Yao**: Investigation, Methodology; Writing—review and editing. **Xiaomei Zhang**: Methodology; Writing—review and editing. **Yuxuan Mao**: Methodology; Writing—review and editing. **Hongping Wei**: Supervision; Methodology; Writing—review and editing. **Jin He**: Conceptualization; Supervision; Methodology; Writing—review and editing. **Hang Yang**: Conceptualization; Supervision; Investigation; Methodology; Methodology; Funding acquisition; Writing—original draft; Writing—review and editing.

Competing interests

The authors declare no competing financial interests.

References

1. Nathan C. 2020. Resisting antimicrobial resistance. Nat Rev Microbiol 18:259-260.
2. Mendelson M, Morris AM, Thursky K, Pulcini C. 2020. How to start an antimicrobial stewardship programme in a hospital. Clin Microbiol Infect 26:447-453.
3. Rawson TM, Ming D, Ahmad R, Moore LSP, Holmes AH. 2020. Antimicrobial use, drug-resistant infections and COVID-19. Nat Rev Microbiol 18:409-410.

734 4. Van Boeckel TP, Pires J, Silvester R, Zhao C, Song J, Criscuolo NG, Gilbert M,
735 Bonhoeffer S, Laxminarayan R. 2019. Global trends in antimicrobial resistance in
736 animals in low- and middle-income countries. Science 365.
737 5. McEwen SA, Collignon PJ. 2018. Antimicrobial Resistance: a One Health Perspective.
738 Microbiol Spectr 6.
739 6. Hernando-Amado S, Coque TM, Baquero F, Martinez JL. 2019. Defining and
740 combating antibiotic resistance from One Health and Global Health perspectives. Nat
741 Microbiol 4:1432-1442.
742 7. Talaat M, Zayed B, Tolba S, Abdou E, Gomaa M, Itani D, Hutin Y, Hajjeh R. 2022.
743 Increasing Antimicrobial Resistance in World Health Organization Eastern
744 Mediterranean Region, 2017-2019. Emerg Infect Dis 28:717-724.
745 8. Brink AJ. 2019. Epidemiology of carbapenem-resistant Gram-negative infections
746 globally. Curr Opin Infect Dis 32:609-616.
747 9. Theuretzbacher U, Outterson K, Engel A, Karlen A. 2020. The global preclinical
748 antibacterial pipeline. Nat Rev Microbiol 18:275-285.
749 10. Lazzaro BP, Zasloff M, Rolff J. 2020. Antimicrobial peptides: Application informed by
750 evolution. Science 368.
751 11. Silver LL. 2016. Appropriate Targets for Antibacterial Drugs. Cold Spring Harb
752 Perspect Med 6.
753 12. Mayer RL, Impens F. 2021. Immunopeptidomics for next-generation bacterial vaccine
754 development. Trends Microbiol 29:1034-1045.
755 13. Luong T, Salabarria AC, Edwards RA, Roach DR. 2020. Standardized bacteriophage
756 purification for personalized phage therapy. Nat Protoc 15:2867-2890.
757 14. De Maesschalck V, Gutierrez D, Paeshuyse J, Lavigne R, Briers Y. 2020. Advanced
758 engineering of third-generation lysins and formulation strategies for clinical
759 applications. Crit Rev Microbiol 46:548-564.
760 15. Korpela K, Helve O, Kolho KL, Saisto T, Skogberg K, Dikareva E, Stefanovic V,
761 Salonen A, Andersson S, de Vos WM. 2020. Maternal Fecal Microbiota Transplantation
762 in Cesarean-Born Infants Rapidly Restores Normal Gut Microbial Development: A
763 Proof-of-Concept Study. Cell 183:324-334 e5.

764 16. Dickey SW, Cheung GYC, Otto M. 2017. Different drugs for bad bugs: antivirulence
765 strategies in the age of antibiotic resistance. Nat Rev Drug Discov 16:457-471.
766 17. Bush K, Bradford PA. 2019. Interplay between beta-lactamases and new beta-lactamase
767 inhibitors. Nat Rev Microbiol 17:295-306.
768 18. Yang H, Xu J, Li W, Wang S, Li J, Yu J, Li Y, Wei H. 2018. Staphylococcus aureus
769 virulence attenuation and immune clearance mediated by a phage lysin-derived protein.
770 EMBO J 37.
771 19. Federici S, Nobs SP, Elinav E. 2021. Phages and their potential to modulate the
772 microbiome and immunity. Cell Mol Immunol 18:889-904.
773 20. Batalha IL, Bernut A, Schiebler M, Ouberai MM, Passemar C, Klapholz C, Kinna S,
774 Michel S, Sader K, Castro-Hartmann P, Renshaw SA, Welland ME, Floto RA. 2019.
775 Polymeric nanobiotics as a novel treatment for mycobacterial infections. J Control
776 Release 314:116-124.
777 21. Farha MA, Brown ED. 2019. Drug repurposing for antimicrobial discovery. Nat
778 Microbiol 4:565-577.
779 22. Jampilek J. 2022. Drug repurposing to overcome microbial resistance. Drug Discov
780 Today 27:2028-2041.
781 23. Torres MDT, Melo MCR, Crescenzi O, Notomista E, de la Fuente-Nunez C. 2022.
782 Mining for encrypted peptide antibiotics in the human proteome. Nat Biomed Eng 6:67-
783 75.
784 24. Ma Y, Guo Z, Xia B, Zhang Y, Liu X, Yu Y, Tang N, Tong X, Wang M, Ye X, Feng J,
785 Chen Y, Wang J. 2022. Identification of antimicrobial peptides from the human gut
786 microbiome using deep learning. Nat Biotechnol 40:921-931.
787 25. Wrighton KH. 2018. Antibacterial drugs: Discovering antibiotics through soil
788 metagenomics. Nat Rev Drug Discov 17:240-241.
789 26. Povolotskaya IS, Kondrashov FA. 2010. Sequence space and the ongoing expansion of
790 the protein universe. Nature 465:922-6.
791 27. Randall JR, DuPai CD, Davies BW. 2022. Discovery of Antimicrobial Peptide
792 Macrocycles Through Bacterial Display. Methods Mol Biol 2371:287-298.

793 28. Das P, Sercu T, Wadhawan K, Padhi I, Gehrmann S, Cipcigan F, Chenthamarakshan V,
794 Strobelt H, Dos Santos C, Chen PY, Yang YY, Tan JPK, Hedrick J, Crain J, Mojsilovic
795 A. 2021. Accelerated antimicrobial discovery via deep generative models and molecular
796 dynamics simulations. Nat Biomed Eng 5:613-623.
797 29. Schmelcher M, Loessner MJ. 2021. Bacteriophage endolysins - extending their
798 application to tissues and the bloodstream. Curr Opin Biotechnol 68:51-59.
799 30. Theuretzbacher U, Piddock LJV. 2019. Non-traditional Antibacterial Therapeutic
800 Options and Challenges. Cell Host Microbe 26:61-72.
801 31. Briers Y, Lavigne R. 2015. Breaking barriers: expansion of the use of endolysins as
802 novel antibacterials against Gram-negative bacteria. Future Microbiol 10:377-90.
803 32. Lai WCB, Chen X, Ho MKY, Xia J, Leung SSY. 2020. Bacteriophage-derived
804 endolysins to target gram-negative bacteria. Int J Pharm 589:119833.
805 33. Lood R, Winer BY, Pelzek AJ, Diez-Martinez R, Thandar M, Euler CW, Schuch R,
806 Fischetti VA. 2015. Novel phage lysin capable of killing the multidrug-resistant gram-
807 negative bacterium Acinetobacter baumannii in a mouse bacteremia model. Antimicrob
808 Agents Chemother 59:1983-91.
809 34. Thandar M, Lood R, Winer BY, Deutsch DR, Euler CW, Fischetti VA. 2016. Novel
810 Engineered Peptides of a Phage Lysin as Effective Antimicrobials against Multidrug-
811 Resistant Acinetobacter baumannii. Antimicrob Agents Chemother 60:2671-9.
812 35. Li C, Jiang M, Khan FM, Zhao X, Wang G, Zhou W, Li J, Yu J, Li Y, Wei H, Yang H.
813 2021. Intrinsic Antimicrobial Peptide Facilitates a New Broad-Spectrum Lysin LysP53
814 to Kill Acinetobacter baumannii In Vitro and in a Mouse Burn Infection Model. ACS
815 Infect Dis 7:3336-3344.
816 36. Kim S, Jin JS, Choi YJ, Kim J. 2020. LysSAP26, a New Recombinant Phage Endolysin
817 with a Broad Spectrum Antibacterial Activity. Viruses 12.
818 37. Yu L, Frank O, Philippe M, Grégory R, Manuel EJ, Stefano M. 2018. In vitro
819 characterization of PlyE146, a novel phage lysin that targets Gram-negative bacteria.
820 PloS one 13.
821 38. Ghose C, Euler CW. 2020. Gram-Negative Bacterial Lysins. Antibiotics (Basel) 9.

822 39. Guo M, Feng C, Ren J, Zhuang X, Zhang Y, Zhu Y, Dong K, He P, Guo X, Qin J. 2017.
823 A Novel Antimicrobial Endolysin, LysPA26, against Pseudomonas aeruginosa. Front
824 Microbiol 8:293.
825 40. Khan FM, Gondil VS, Li C, Jiang M, Li J, Yu J, Wei H, Yang H. 2021. A Novel
826 Acinetobacter baumannii Bacteriophage Endolysin LysAB54 With High Antibacterial
827 Activity Against Multiple Gram-Negative Microbes. Front Cell Infect Microbiol
828 11:637313.
829 41. Briers Y, Walmagh M, Lavigne R. 2011. Use of bacteriophage endolysin EL188 and
830 outer membrane permeabilizers against Pseudomonas aeruginosa. J Appl Microbiol
831 110:778-85.
832 42. Walmagh M, Boczkowska B, Grymonprez B, Briers Y, Drulis-Kawa Z, Lavigne R. 2013.
833 Characterization of five novel endolysins from Gram-negative infecting bacteriophages.
834 Appl Microbiol Biotechnol 97:4369-75.
835 43. Oliveira H, Thiagarajan V, Walmagh M, Sillankorva S, Lavigne R, Neves-Petersen MT,
836 Kluskens LD, Azeredo J. 2014. A thermostable Salmonella phage endolysin, Lys68,
837 with broad bactericidal properties against gram-negative pathogens in presence of weak
838 acids. PLoS One 9:e108376.
839 44. Plotka M, Kapusta M, Dorawa S, Kaczorowska AK, Kaczorowski T. 2019. Ts2631
840 Endolysin from the Extremophilic Thermus scotoductus Bacteriophage vB_Tsc2631 as
841 an Antimicrobial Agent against Gram-Negative Multidrug-Resistant Bacteria. Viruses
842 11.
843 45. Raz A, Serrano A, Hernandez A, Euler CW, Fischetti VA. 2019. Isolation of phage lysins
844 that effectively kill Pseudomonas aeruginosa in mouse models of lung and skin infection.
845 Antimicrobial Agents and Chemotherapy.
846 46. Lavigne R, Briers Y, Hertveldt K, Robben J, Volckaert G. 2004. Identification and
847 characterization of a highly thermostable bacteriophage lysozyme. Cell Mol Life Sci
848 61:2753-9.
849 47. Briers Y, Lavigne R, Plessers P, Hertveldt K, Hanssens I, Engelborghs Y, Volckaert G.
850 2006. Stability analysis of the bacteriophage KMV lysin gp36C and its putative role
851 during infection. Cellular and Molecular Life ences CMLS 63:1899-1905.

852 48. Tsugita A, Inouye M, Terzaghi E, Streisinger G. 1968. Purification of Bacteriophage T4
853 Lysozyme. Journal of Biological Chemistry 243.
854 49. Schmelcher M, Waldherr F, Loessner MJ. 2012. Listeria bacteriophage peptidoglycan
855 hydrolases feature high thermoresistance and reveal increased activity after divalent
856 metal cation substitution. Applied Microbiology and Biotechnology 93:633-643.
857 50. Knowles B, Silveira CB, Bailey BA, Barott K, Cantu VA, Cobian-Guemes AG,
858 Coutinho FH, Dinsdale EA, Felts B, Furby KA, George EE, Green KT, Gregoracci GB,
859 Haas AF, Haggerty JM, Hester ER, Hisakawa N, Kelly LW, Lim YW, Little M, Luque
860 A, McDole-Somera T, McNair K, de Oliveira LS, Quistad SD, Robinett NL, Sala E,
861 Salamon P, Sanchez SE, Sandin S, Silva GG, Smith J, Sullivan C, Thompson C, Vermeij
862 MJ, Youle M, Young C, Zgliczynski B, Brainard R, Edwards RA, Nulton J, Thompson
863 F, Rohwer F. 2016. Lytic to temperate switching of viral communities. Nature 531:466-
864 70.
865 51. Miller-Ensminger T, Garretto A, Brenner J, Thomas-White K, Zambom A, Wolfe AJ,
866 Putonti C. 2018. Bacteriophages of the Urinary Microbiome. J Bacteriol 200.
867 52. Keen EC, Dantas G. 2018. Close Encounters of Three Kinds: Bacteriophages,
868 Commensal Bacteria, and Host Immunity. Trends Microbiol 26:943-954.
869 53. Lagier JC, Dubourg G, Million M, Cadoret F, Bilen M, Fenollar F, Levasseur A, Rolain
870 JM, Fournier PE, Raoult D. 2018. Culturing the human microbiota and culturomics. Nat
871 Rev Microbiol 16:540-550.
872 54. Kilcher S, Studer P, Muessner C, Klumpp J, Loessner MJ. 2018. Cross-genus rebooting
873 of custom-made, synthetic bacteriophage genomes in L-form bacteria. Proc Natl Acad
874 Sci U S A 115:567-572.
875 55. Arndt D, Marcu A, Liang Y, Wishart DS. 2019. PHAST, PHASTER and PHASTEST:
876 Tools for finding prophage in bacterial genomes. Brief Bioinform 20:1560-1567.
877 56. Song W, Sun HX, Zhang C, Cheng L, Peng Y, Deng Z, Wang D, Wang Y, Hu M, Liu W,
878 Yang H, Shen Y, Li J, You L, Xiao M. 2019. Prophage Hunter: an integrative hunting
879 tool for active prophages. Nucleic Acids Res 47:W74-W80.

880 57. Siren K, Millard A, Petersen B, Gilbert MTP, Clokie MRJ, Sicheritz-Ponten T. 2021.
881 Rapid discovery of novel prophages using biological feature engineering and machine
882 learning. NAR Genom Bioinform 3:lqaa109.
883 58. Zhang BZ, Cai J, Yu B, Xiong L, Lin Q, Yang XY, Xu C, Zheng S, Kao RY, Sze K, Yuen
884 KY, Huang JD. 2017. Immunotherapy Targeting Adenosine Synthase A Decreases
885 Severity of Staphylococcus aureus Infection in Mouse Model. J Infect Dis 216:245-253.
886

Supplemental Materials For

Dimer-monomer transition defines a novel hyper-thermostable peptidoglycan hydrolase mined from bacterial proteome

Li Zhang[1,#], Fen Hu[2,#], Zirong Zhao[1,#], Xinfeng Li[3], Mingyue Zhong[3], Jiajun He[1], Fangfang Yao[4], Xiaomei Zhang[1], Yuxuan Mao[1], Hongping Wei[2], Jin He[1,*], Hang Yang[3,5,6,*]

Table S1. Physicochemical properties of putative antimicrobial peptides in PHAb10 and PHAb11

Parameter	Amino acid sequence	Molecular weight (kDa)	pI	Negatively /positively charged residues	Net charge	Instability index	Aliphatic index	GRAVY
P10-CP	NKGDYQGAADQFLVWNKAGGKVMKGLVRRREAERALFLKK	4550	10.37	4/10	6	39.66	73.25	-0.733
P11-CP	NKGDYKGAADQFLVWNKAGGKVLKGLVRRREAERALFLKK	4532	10.45	4/11	7	35.41	83.00	-0.695
P11-NP	MTTKPFFDAARVIAGGKLTQAQVDELNKVVNKLAPG	3829	9.52	3/5	2	19.74	89	-0.053

Positively charged amino acids are labeled in red.

GRAVY: Grand average of hydropathicity.

Table S2. Data collection and refinement statistics of PHAb8, PHAb10, and PHAb11 structures

Parameters	PHAb10	PHAb11	PHAb8
Data collection			
Wavelength (Å)	0.9793	0.9793	0.9793
Space group	$P\ 1\ 2_1\ 1$	$P\ 2\ 2\ 2_1$	$C\ 2\ 2\ 2_1$
Cell dimensions			
a, b, c (Å)	31.86 73.77 78.62	50.01 54.9 161.31	79.03 156.98 47.26
α, β, γ (°)	90.00 93.02 90.00	90 90 90	90 90 90
Resolution range (Å)	31.82 - 1.52 (1.574 - 1.52)	36.62 - 2.27 (2.351 - 2.27)	32.06 - 2.4 (2.486 - 2.4)
Unique reflections	55245 (5468)	21246 (2049)	11880 (1048)
Multiplicity	6.8 (6.5)	12.3 (12.4)	12.9 (13.2)
Completeness (%)	98.86 (98.17)	99.65 (99.80)	94.57 (88.22)
Mean I/sigma I	18.36 (1.67)	14.54 (2.02)	10.50 (1.53)
Wilson B-factor ($Å^2$)	24.27	31.87	37.86
R_{merge}	0.04816 (1.097)	0.2869 (1.486)	0.213 (1.914)
R_{meas}	0.0522 (1.192)	0.2999 (1.55)	0.2219 (1.991)
$CC_{1/2}$	0.999 (0.788)	0.992 (0.747)	0.996 (0.579)
Refinement			
Resolution (Å)	31.82 - 1.52	36.62 - 2.27	32.06 - 2.4
R_{work}	0.1921 (0.3344)	0.2483 (0.3092)	0.2520 (0.3560)
R_{free}	0.2151 (0.3653)	0.2660 (0.3670)	0.2849 (0.4396)
Ligands	0	18	17
Rmsd from ideal			
Bond lengths (Å)	0.004	0.005	0.010
Bond angles (°)	0.62	0.75	1.18
Ramachandran plot			
Favored (%)	98.97	98.25	95.81
Allowed (%)	1.03	1.75	4.19
Outliers (%)	0.00	0.00	0.00
Average B-factor	32.18	37.23	52.84

PDB Code	7YKU	8HDQ	8HEM

Statistics for the highest-resolution shell are shown in parentheses.

Table S3. T4L-like lysozymes with characterized structures

Protein	Catalytic Residues			PDB ID
PHAb8	Glu74	Asp83	Thr89	8HEM
PHAb10	Glu17	Asp26	Thr32	7YKU
PHAb11	Glu52	Asp61	Thr67	8HDQ
AcLys	Glu64	Asp73	Thr79	6ET6
LysF1	Glu15	Asp24	Thr30	7M5I
SpmX-Mur-*Ae*	Glu18	Leu27	Met33	6H9D
P22	Glu16	Asp25	Thr31	2ANX
R21	Glu35	Asp44	Thr50	3HDE
HEWL	Glu35	Asp52		4HPI
GEWL	Glu73			153L
phage lambda lytic transglycosylase	Glu19			1D9U
T4L	Glu11	Asp20	Thr26	1LYD

Table S4. Intermolecular interactions of PHAb10 dimer

PHAB10 dimer	Serial number	Donor (atom 1)	Acceptor (atom 2)	Distance/Å	Force
Head-supporting force	1	R20.NH1 (Chain A)	G129.O (Chain B)	3.5	H-bond
	2	T104.N (Chain B)	G27.O (Chain A)	3.1	H-bond
	3	T104.OG1 (Chain B)	G27.O (Chain A)	3.5	H-bond
Midbody-supporting force	4	E97.N (Chain B)	G128.O (Chain A)	2.9	H-bond
	5	K67.NZ (Chain B)	G129.O (Chain A)	2.9	H-bond
Tail-supporting force	6	K133.NZ (Chain A)	D26.O (Chain B)	2.9	H-bond
	7	R137.NH1 (Chain A)	G27.O (Chain B)	2.7	H-bond

Table S5. PHAb10 variants

Native amino acids (Chain A)	Substituted amino acids	Mutant name
R20, G27	R20I, G27D	R20I/G27D
G128, G129	G128D, G129D	G128D/G129D
G27, R137	G27D, R137I	G27D/R137I
K133, R137	K133A, R137I	K133A/R137I
R20, G27, K67, G128, K133, R137	R20E, G27T, K67W, G128N, K133A, R137N	PHAb10-mut

Table S6 Bacterial strains used in this work.

Strain	Source	Strain	Source
Acinetobacter baumanni		***Klebsiella pneumoniae***	
ABA3437	WIV[b]	KP21	WIV[b]
CRAB2	WIV[b]	KP22	WIV[b]
CRAB13	WIV[b]	KP23	WIV[b]
CRAB36	WIV[b]	KP24	WIV[b]
CRAB27	WIV[b]	KP26	WIV[b]
CRAB28	WIV[b]	KP27	WIV[b]
CRAB22	WIV[b]	KP28	WIV[b]
CRAB26	WIV[b]	KP602	WIV[b]
CRAB140	WIV[b]	KP605	WIV[b]
CRAB143	WIV[b]	KP607	WIV[b]
CRAB147	WIV[b]	***Pseudomonas aeruginosa***	
Escherichia coli		PAE2555	WIV[b]
E. coli 100	WIV[b]	PAE1	WIV[b]
E. coli BL21	WIV[b]	PAE2	WIV[b]
E. coli O91	WIV[b]	PAE52	WIV[b]
E. coli O97	WIV[b]	PAE53	WIV[b]
E. coli O149	WIV[b]	PAE2139	WIV[b]
E. coli O517	WIV[b]	PAE2169	WIV[b]
E. coli MS31	WIV[b]	PAE2176	WIV[b]
E. coli MS33	WIV[b]	PAE2703	WIV[b]
E. coli MS28	WIV[b]	PAE3223	WIV[b]
E. coli MS34	WIV[b]	PA2-3121	WIV[b]
Staphylococcus aureus		PA2-3283	WIV[b]
S. aureus N315	WIV[b]	PA2-3763	WIV[b]
S. aureus RN4220	WIV[b]	PA2-3965	WIV[b]
S. aureus NF71	WIV[b]	***Streptococcus***	
S. aureus 25923	WIV[b]	*S. pneumoniae* 17NS26	HPPH[a]
Enterococcus faecalis		*S. agalactiae* 12	WIV[b]
E. faecalis 493	WIV[b]	*S. agalactiae* C001	WIV[b]
E. faecalis 29212	ATCC[c]	*S. dysgalactiae* 35666	ATCC[c]
E. faecalis 51299	WIV[b]	*S. pyogenes* 12344	ATCC[c]
E. faecalis 571-2	WIV[b]	*S. mutans* 159	WIV[b]
		S. Suis 1	HUAHE[d]

a: Isolated from Henan Provincial People's Hospital, Zhengzhou, China.

b: Obtained from Wuhan Institute of Virology, Chinese Academy of Sciences, Wuhan, China.

c: Purchased from Guangdong Culture Collection Center, China.

d: Obtained from Henan University of Animal Husbandry and Economy, Zhengzhou, China.

Table S7. Primers used in this study.

Primer	Sequence (5'-3')
P10-Lys-F	ctttaagaaggagatataccATGggcatgagcaaaaccaccagt
P10-Lys-R	gtggtggtgctcgagCAGtttttcagcaggg
P11-N-F	agaaggagatataccATGggcatgaccaccaaaccgtttttgatgcag
P11-N-R	gtggtggtgctcgagCAGcagtttcagcagggtgcta
P11-C-F1	aactttaagaaggagatataccatgggtggtaaaaccacc
P11-C-R1	ggtggtggtgctcgagtttttcagaaacagtgcacg
P11-C-F2	aactcgagcaccaccaccaccaccac
P11-C-R2	ggtatatctccttcttaaagttaaacaaaattatttctagag
K133AR137I-F1	tttgtttaactttaagaaggagatataccatgggcatgagcaaaaccacc
K133AR137I-R1	acgacggataaccagaccggccataactttaccacc
K133AR137I-F2	tggccggtctggttatccgtcgtgaagcagaac
K133AR137I-R2	gctcatgcccatggtatatctccttcttaaagttaaacaaaattatttc
R20IG27D-F1	accaccagtaatgcaggtctgaatctgatcaaaggttttgaaggtaaaatcctgaatgc
R20IG27D-R1	gtgccaaaaccaatggtccaaacaccaacatcatcatcataggcattcaggattttacc
R20IG27D-F2	ccattggttttggcaccatcaaatatccgaatggtgttcg
R20IG27D-R2	cctgcattactggtggttttgctcatgcccatggtatatc
G128DG129D-F1	atgagcaaaaccaccagtaatgcaggtctgaatctgatcaaag
G128DG129D-R1	aactttatcatcggctttattccaaaccagaaactgatctgctgc
G128DG129D-F2	aagccgatgataaagttatgaaaggtctggttcgtcgtcg
G128DG129D-R2	actggtggttttgctcatgcccatggtatatctccttc
G27DR137I-F1	tgatgatgttggtgtttggaccattggttttggcacc
G27DR137I-R1	tctgcttcacgacggataaccagacctttcataactttaccac
G27DR137I-F2	ggttatccgtcgtgaagcagaacgtgcactg
G27DR137I-R2	ccaaacaccaacatcatcatcataggcattcaggcg

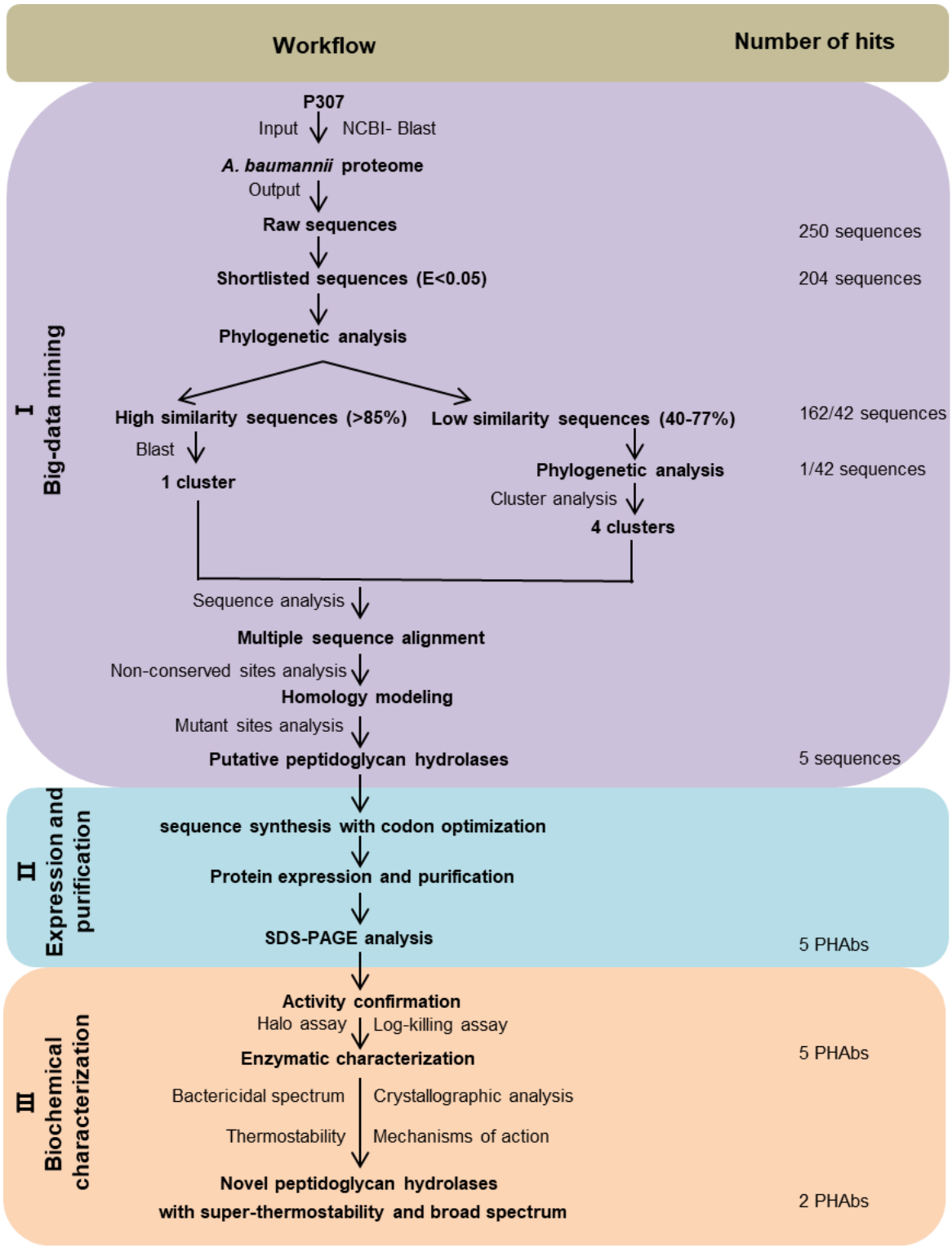

Figure S1. Workflow of an integrated system for the exploitation of peptidoglycan hydrolases. Three distinct phases of the workflow were highlighted in different colors: (I) Screening of peptidoglycan hydrolases using cationic peptides P307 as templates (yellow). (II) Expression and purification of protein (blue). (III) Biochemical characterization (green).

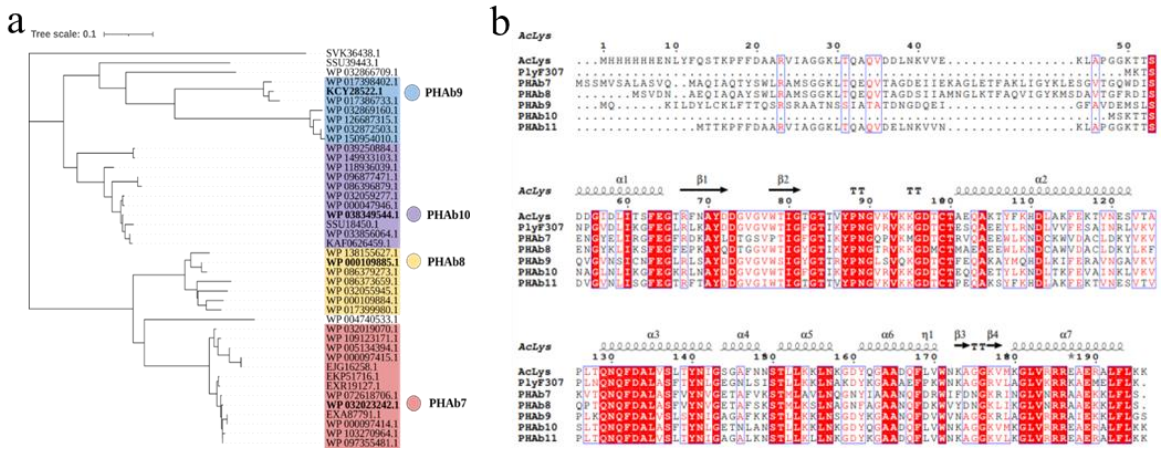

Figure S2. Selection of five putative peptidoglycan hydrolases. (a) Phylogenetic tree of *A. baumannii* peptidoglycan hydrolases homolog to P307. (b) Multiple sequence alignment of PHAb7, PHAb8, PHAb9, PHAb10, PHAb11, PlyF307, and AcLys using MEGAX software and ClustalW algorithm. Secondary structures were annotated by Espript 3.0 website.

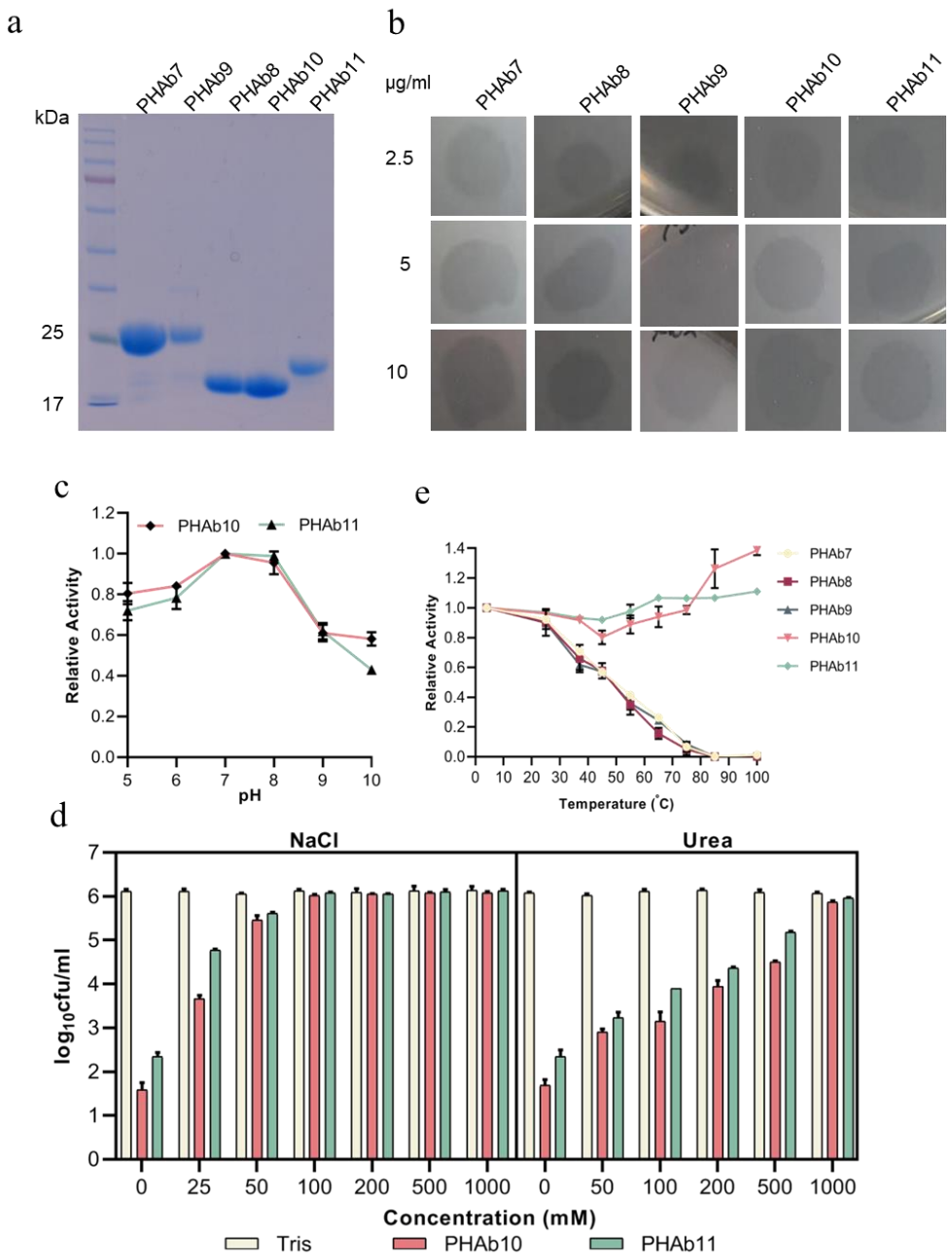

Figure S3. Testing of bactericidal activity of screened putative peptidoglycan hydrolases. (a) Purified proteins were analyzed on a 12% SDS-PAGE gel. M: standard protein marker. (b) Halos of five PHAbs on *A. baumannii* 3437 lawns. The concentrations of each peptidoglycan hydrolase were 2.5 μg/ml, 5 μg/ml, and 10 μg/ml. (c) pH stability of PHAb10 and PHAb11. Log-phase *A. baumannii* 3437 cells were incubated with 50 μg/ml peptidoglycan hydrolases at the indicated pH conditions for 1 hour at 37°C. pH buffer: 20 mM Boric acid mixed with 20 mM phosphoric acid in equal volumes and adjusted to different pH values with HCl. (d) Log-phase *A. baumannii* 3437 cells incubated with 50 μg/ml of each peptidoglycan hydrolase at different concentrations of NaCl (left) and urea (right) for 1 hour at 37°C in 20 mM Tris-HCl (pH 7.4). (e) Relative activity of five PHAbs against *A. baumannii* 3437 after 1 hour storage at different temperatures. In all cases, viable bacteria were counted by serial dilution and plating assays. Experiments were carried out in triplicate; error bars represent standard deviation.

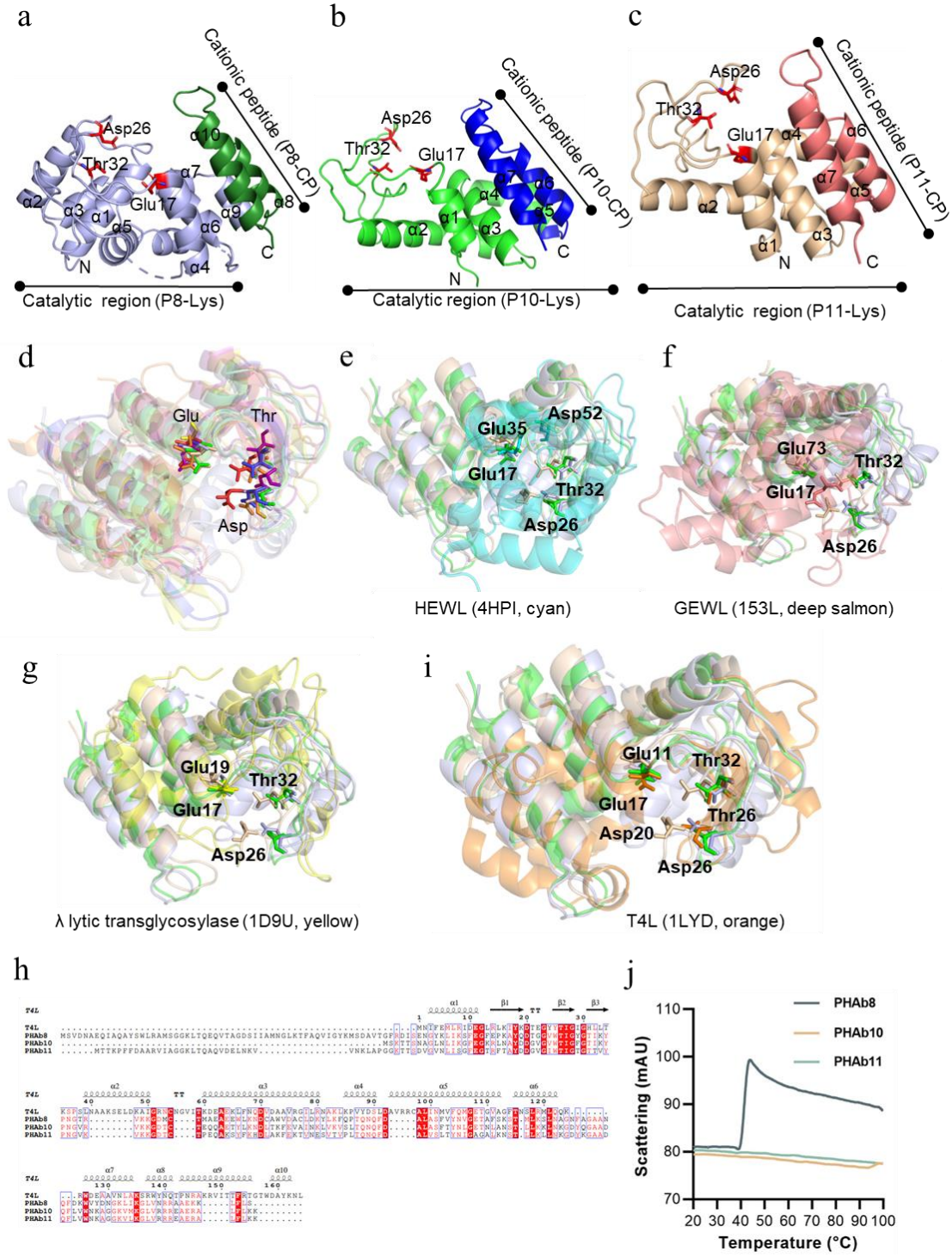

Figure S4. Structural analysis of PHAb8, PHAb10, and PHAb11. (a-c) Structures of monomeric PHAb8 (a), PHAb10 (b), and PHAb11 (c). (d) Structural superposition of PHAb8, PHAb10, PHAb11 and five classical T4L-like lysozymes that share high similarity from Dali search. PHAb8 is shown in light blue, PHAb10 in green, PHAb11 in wheat, AcLys in red, LysF1 in blue, SpmX-Mur-*Ae* in yellow, P22 in purple, and R21 in orange. (e-h) Structural alignment of PHAb8, PHAb10, PHAb11 with various lysozymes including HEWL (e, cyan), GEWL (f, deep salmon), phage lambda lytic transglycosylase (g, yellow) and T4 lysozyme (h, orange). Residues in the conservative catalytic triad are shown as sticks. (j) Scattering profiles of PHAb8, PHAb10, and PHAb11 at different temperatures determined by NanoDSF.

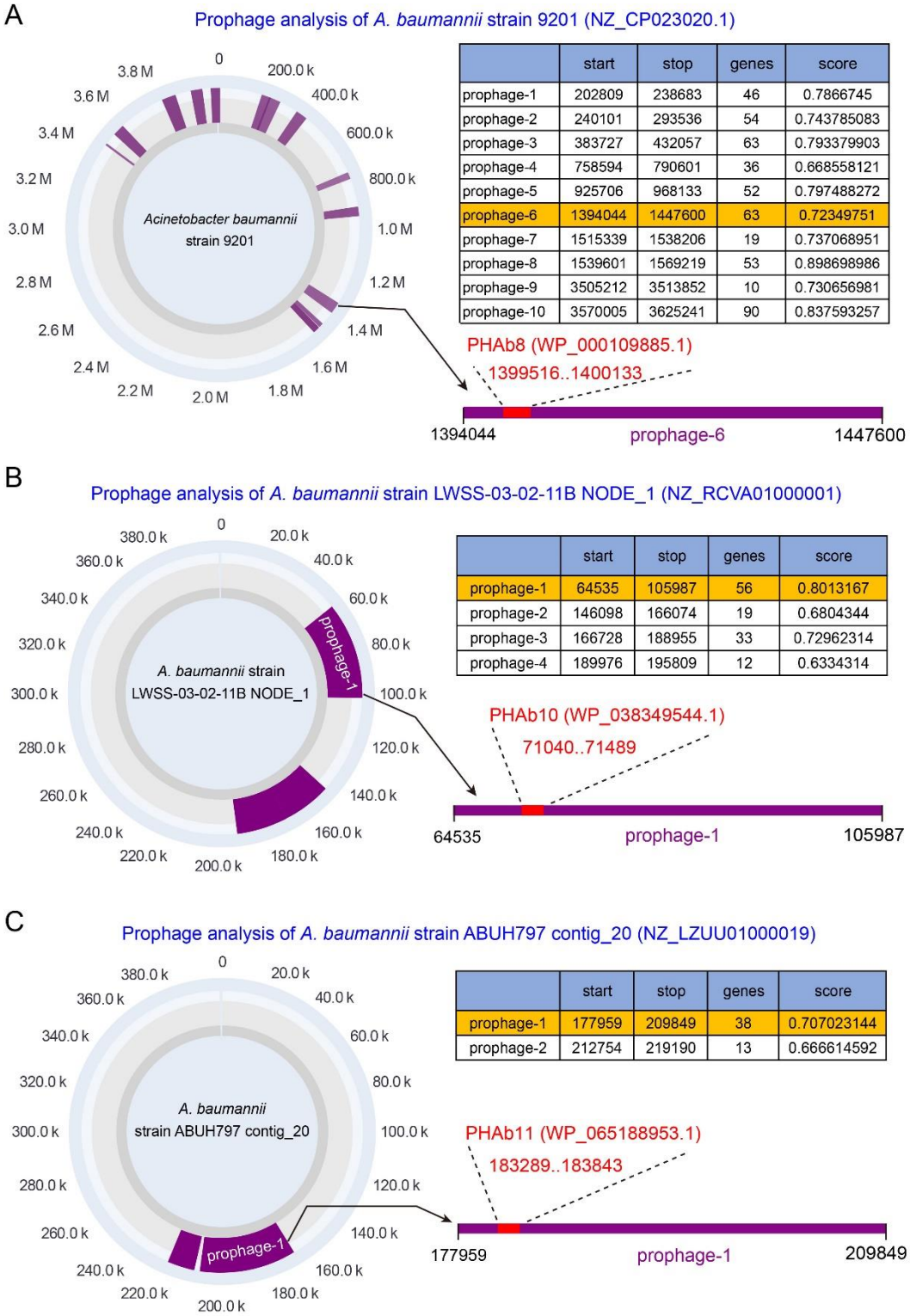

	start	stop	genes	score
prophage-1	202809	238683	46	0.7866745
prophage-2	240101	293536	54	0.743785083
prophage-3	383727	432057	63	0.793379903
prophage-4	758594	790601	36	0.668558121
prophage-5	925706	968133	52	0.797488272
prophage-6	1394044	1447600	63	0.72349751
prophage-7	1515339	1538206	19	0.737068951
prophage-8	1539601	1569219	53	0.898698986
prophage-9	3505212	3513852	10	0.730656981
prophage-10	3570005	3625241	90	0.837593257

	start	stop	genes	score
prophage-1	64535	105987	56	0.8013167
prophage-2	146098	166074	19	0.6804344
prophage-3	166728	188955	33	0.72962314
prophage-4	189976	195809	12	0.6334314

	start	stop	genes	score
prophage-1	177959	209849	38	0.707023144
prophage-2	212754	219190	13	0.666614592

Figure S5. Prophage analysis of PHAbs. PHAb8, PHAb10, and PHAb11 encoding sequences were retrieved from *A. baumannii* strain 9201, *A. baumannii* strain LWSS-03-02-11B, and *A. baumannii* strain ABUH797 and analyzed by PhageBoost tool. Results revealed that all three genes are indeed located within prophage regions.

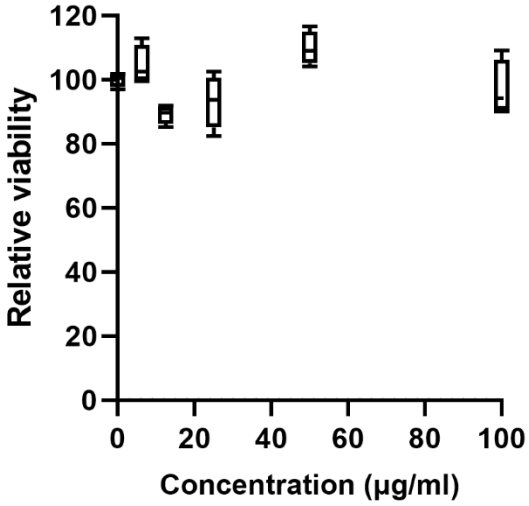

Figure S6. Relative viability of HepG2 cells exposed to different concentrations of PHAb10. Cells were cultured in DMEM supplemented with 10% fetal bovine serum, 1% penicillin, and 1% streptomycin for 24 h. After the cells were exposed to a series of concentrations of PHAb10 (0, 6.25, 12.5, 25, 50, and 100 μg/ml) for another 24 h, the relative viability of the cells after each treatment was determined by the CCK-8 assay.